Asia-Pacific Journal of Atmospheric Sciences (2021) 57:717–739
https://doi.org/10.1007/s13143-021-00228-3

Online ISSN 1976-7951
Print ISSN 1976-7633

ORIGINAL ARTICLE

Assessment of Ocean-Atmosphere Interactions for the Boreal Summer Intraseasonal Oscillations in CMIP5 Models over the Indian Monsoon Region

Gopinadh Konda[1] · Naresh Krishna Vissa[1]

Received: 28 July 2020 / Revised: 4 January 2021 / Accepted: 13 January 2021 / Published online: 26 January 2021

Abstract

The boreal summer intraseasonal oscillations (BSISO) are the prominent features of South Asian summer monsoon and mainly governed by the internal atmospheric dynamics and air-sea interactions. The present study aims to understand and evaluate the relationship between the convection and the associated air-sea interactions during the BSISO over the Indian monsoon region. To accomplish this, the present study utilizes observations and the 22 general circulation model (GCM) simulations from the Coupled Model Intercomparison Project Phase 5 (CMIP5). Representation of Indian monsoon season rainfall, sea surface temperature (SST) and latent heat fluxes in CMIP5 models such as climatological and intraseasonal are assessed using Global Precipitation Climatology Project rainfall by Taylor diagram metric. Results suggest that the majority of CMIP5 models simulated the northward propagation of precipitation and zonal wind at 850 hPa. However, models bias of BSISO variance shows significant spatial heterogeneity over the regions of the Arabian Sea (AS), Sub-Continent of India (SCI) and Bay of Bengal (BoB). The CMIP5 model which shows large biases in the mean state is degrading the northward propagation of BSISO. The phase relationship of ocean (land) and atmospheric interactions are diagnosed with lead-lag regression analysis. On ISO timescales over north Indian Ocean (NIO) convection leads the turbulent fluxes and westerly winds by a week. However, the majority of the models shows large uncertainty to represent this prominent feature over AS and SCI. Further, improper representation of the lead-lag relationship of SST and precipitation on ISO scales over the AS, BoB, and NIO in the CMIP5 models are attributing for significant bias variances. The present study advocates that BSISO propagation in CMIP5 models is mainly attributing from the internal atmospheric dynamics and air-sea interactions. However, for the realistic amplitude simulation of BSISO, proper representation of air-sea feedback mechanisms is crucial in CMIP5 models. The present study further suggests that the oceanic feedback processes of the CMIP5 models need to be improved for the accurate prediction of the intraseasonal variations.

Keywords Indian summer monsoon · Boreal summer intraseasonal oscillations · Air-sea interactions · CMIP5 models

1 Introduction

The monsoon is one of the key components of the seasonal cycle, which are characterized with the strong reversal of winds in the lower troposphere, most torrential rainfall and significant heat source in the tropical atmosphere (Webster et al. 1998; Gadgil 2003; Jiang and Li 2011; Jiang et al. 2013). Most of the regions over the Indian subcontinent receives significant amount of annual rainfall (~80%) during the Indian summer monsoon (ISM) season (June to September) (e.g. Parthasarathy et al. 1994; Sperber et al. 2013; DeMott et al. 2015; Ramu et al. 2018; Chowdary et al. 2019; Attada et al. 2019). The ISM exhibits variability on a widespread of spatial and temporal scales (e.g. Krishnamurthy and Achuthavarier 2012; Konda and Vissa 2019). The active and break phases of rainfall are the characteristic feature of the ISM, which is primarily modulated by the tropical intraseasonal oscillations (TISO) such as northward propagating boreal summer intraseasonal oscillations (BSISO) and eastward propagating Madden Julian Oscillations (MJO) (e.g. Gadgil 2003; Goswami et al. 2006;

Responsible Editor: June-Yi Lee.

✉ Naresh Krishna Vissa
vissan@nitrkl.ac.in; vissanaresh@gmail.com

[1] Department of Earth and Atmospheric Sciences, National Institute of Technology Rourkela, Dist: Sundargarh, Odisha 769008, India

Abhik et al. 2013; Kikuchi et al. 2012; Lee et al. 2013; Anandh et al. 2018; Gao et al. 2019). The BSISO is predominant during boreal summer (May–October); however, the MJO dominates during winter (December–April) (e.g. Kikuchi et al. 2012; Lee et al. 2013).

Several studies suggested that the internal atmospheric dynamics and the processes such as easterly vertical wind shear, moisture, convection mechanism (e.g. Jiang et al. 2004; Ajayamohan et al. 2011; Liu et al. 2018), Rossby wave emanation from the equatorial convection (e.g. Wang and Xie 1997; Karmakar and Krishnamurti 2019), convective momentum transport induced by cumulus convection (e.g. Kang et al. 2010; Liu et al. 2015), shallow convection (e.g. Liu et al. 2018), cloud hydrometeors and associated mid-tropospheric heating (e.g. Abhik et al. 2013) are responsible for the northward propagation of BSISO. The interaction between rainfall and land surface sensible heat flux favours the northward propagation (Webster 1983). Recent observations and modelling studies shown that the air-sea interactions modify the dynamics of BSISO amplitude and northward propagation (Sengupta et al. 2001; Kemball-Cook et al. 2002; Webster et al. 2002; Hendon 2005; Roxy and Tanimoto 2007; Roxy et al. 2013; Sharmila et al. 2013; Sharmila et al. 2014a; Zhang et al. 2018; Wang et al. 2018; Gao et al. 2019). Karmakar and Misra (2020) identified the intensity of ISOs are stronger over Bay of Bengal (BoB) than the Arabia Sea (AS). Sengupta et al. (2001) suggested that the high intraseasonal variability of sea surface temperature (SST) in the tropical oceans is crucial for the northward propagating BSISO. The intraseasonal variability of SST over the Indian Ocean attributed to variations of the surface sensible heat flux and solar radiation (Sengupta and Ravichandran 2001). On the other hand, the change in the atmosphere reflects in the SST changes over these regions (Roxy and Tanimoto 2012; Wu 2010). Zhang and McPhaden (1995) established the relationship between SST and latent heat fluxes (LHFs) on intraseasonal time scales by using observations from the Tropical Ocean Global Atmosphere Tropical Atmosphere-Ocean (TOGA-TAO) moored buoy over the equatorial western Pacific Ocean. Kemball-Cook and Wang (2001) identified that the prediction of enhanced surface evaporation occurs ~10 days prior to surface convergence and precipitation anomalies over the NIO, suggesting the important role of air-sea interactions in dynamics of BSISO.

Several observations and general circulation models (GCMs), for example, atmosphere-only and atmosphere and ocean coupled models concluded that the convection-circulation and atmosphere-ocean coupled interactions are crucial for the northward propagation of the BSISO (e.g. Seo et al. 2007; Wang et al. 2009; Ajayamohan et al. 2011; Lee and Wang 2014; Fu and Wang 2004; Kang et al. 2010). The state-of-the-art models still have difficulties in predicting the initiation, development, and termination of BSISO (e.g. Kemball-Cook et al. 2002; Fu and Wang 2004; Fu et al. 2007; Seo and Wang 2010; Ajayamohan et al. 2011; Sharmila et al. 2014b; Neena et al. 2017). The fully coupled National Centers for Environmental Prediction (NCEP) climate forecast system model (CFS) simulations suggest that the realistic representation of seasonal SST is essential for realistic prediction of BSISO (e.g. Seo et al. 2007). The incorporation of diurnal variations of SSTs and solar radiation in the GCMs is also an essential factor for BSISO simulation (Danabasoglu et al. 2006; Ham et al. 2010; Oh et al. 2013). Over the Indian monsoon region, the results of NCEP coupled CFS, and atmosphere-only Global Forecast System (GFS) simulations suggest that the inclusion of an interactive ocean surface is necessary for the maintenance of northward propagating BSISO; however, GFS model fail to simulate the convection beyond 12°N from equator (e.g. Wang et al. 2009). Klingaman et al. (2011) analyzed the impact of higher temporal and spatial resolution coupled GCMs on the BSISO during ISM season, and their findings suggest that sub-daily forcing can produce the stronger quadrature relationship between the upper-ocean temperature and convection anomalies. In summary, recent numerous modelling studies indicate that ocean-atmosphere coupling is necessary for the improvement of BSISO simulation and prediction (e.g. DeMott et al. 2013; Abhik et al. 2013; Jiang et al. 2013).

The world climate modelling organizations have conducted Coupled Model Intercomparison Project phase5 (CMIP5) in preparation for the Intergovernmental Panel on Climate Change (IPCC) Fifth Assessment Report (AR5) (e.g. Taylor et al. 2012; Sperber et al. 2013). Many studies have shown that CMIP5 models have variable skill in simulating the ISM variability (Jain et al. 2019; Jena et al. 2016; Azad and Rajeevan 2016; Choudhary et al. 2019; Preethi et al. 2019). The CMIP5 models are different in many aspects (e.g. subgrid-scale parameterizations, aerosol representation, cloud physics, atmospheric chemistry and oceanic properties). Some models share the same parameterizations of processes, numerical approximations, or even the same ocean, sea ice, land, or atmospheric components, possibly leading to similar biases (Knutti and Sedláček 2013; Frolicher et al. 2015; Pathak et al. 2019). For example, the GFDL developed two coupled carbon cycle climate Earth system models (ESMs), which differ mainly in their ocean model formulation and, principally, in their vertical coordinate. GFDL-ESM2M, is based on the Modular Ocean Model, version 4.1 (MOM4p1; Griffies et al. 2009), where the advective terms and physical parameterizations are

Table 1 Details of the 22 CMIP5 Models, that participated in the CMIP5 project

Modeling Institution or Group	Model name	Horizantal Resolution (lon×lat) and Vertical levels	Ensemble Member
Commonwealth Scientific and Industrial Research Organization (CSIRO) andBureau of Meteorology (BOM), Australia	ACCESS1.0	1.87°×1.25°, L38	r1i1p1
Commonwealth Scientific and Industrial Research Organization (CSIRO) andBureau of Meteorology (BOM), Australia	ACCESS1.3	1.87°×1.25°, L38	r1i1p1
Canadian Centre for Climate Modelling and Analysis, Canada	CanESM2		r1i1p1
Centro Euro-Mediterraneo per I Cambiamenti Climatici, Italy	CMCC-CESM	T39, L31	r1i1p1
Centro Euro-Mediterraneo per I Cambiamenti Climatici, Italy	CMCC-CMS	T63, L95	r1i1p1
Centre National de Recherches Meteorologiques / Centre Europeen de Recherche etFormation Avancees en Calcul Scientifique, France	CNRM-CM5	T127, L31	r1i1p1
Geophysical Fluid Dynamics Laboratory, USA	GFDL-CM3	2.5°×2°, L48	r1i1p1
Geophysical Fluid Dynamics Laboratory, USA	GFDL-ESM2G	2.5°×2°, L24	r1i1p1
Geophysical Fluid Dynamics Laboratory, USA	GFDL-ESM2M	2.5°×2°, L24	r1i1p1
Institute for Numerical Mathematics, Russia	INM-CM4	2°×1.5°, L21	r1i1p1
Institut Pierre-Simon Laplace, France	IPSL-CM5A-LR	3.75°×1.87°, L39	r1i1p1
Institut Pierre-Simon Laplace, France	IPSL-CM5A-MR	2.5°×1.25°, L39	r1i1p1
Institut Pierre-Simon Laplace, France	IPSL-CM5B-LR	3.75°×1.87°, L39	r1i1p1
Atmosphere and Ocean Research Institute (The University of Tokyo), National Institutefor Environmental Studies, and Japan Agency for Marine-Earth Science and Technology, Japan	MIROC5	T85, L40	r1i1p1
Japan Agency for Marine-Earth Science and Technology, Atmosphere and OceanResearch Institute (The University of Tokyo), and National Institute for EnvironmentalStudies, Japan	MIROC-ESM	T42, L80	r1i1p1
Japan Agency for Marine-Earth Science and Technology, Atmosphere and OceanResearch Institute (The University of Tokyo), and National Institute for EnvironmentalStudies, Japan	MIROC-ESM-CHEM	T42, L80	r1i1p1
Max Planck Institute for Meteorology (MPI-M), Germany	MPI-ESM-LR	T63, L47	r1i1p1
Max Planck Institute for Meteorology (MPI-M), Germany	MPI-ESM-MR	T63, L95	r1i1p1
Max Planck Institute for Meteorology (MPI-M), Germany	MPI-ESM-P	T63, L47	r1i1p1
Meteorological Research Institute, Japan	MRI-CGCM3	T159, L48	r1i1p1
Meteorological Research Institute, Japan	MRI-ESM1	1°×0.5°, L50	r1i1p1
Norwegian Climate Centre, Norway	NorESM1-M	2.5°×1.87°, L39	r1i1p1

computed with a vertical coordinate. However, GFDL-ESM2G, is based on the Generalized Ocean Layer Dynamics model (Hallberg and Adcroft 2009), which employs an isopycnal r-coordinate. IPSL-CM5A-LR, IPSL-CM5A-MR and IPSL-CM5B-LR were developed by slight modification in resolution and atmospheric component; MIROC-ESM and MIROC-ESM-CHEM differ in ocean biogeochemistry and atmospheric chemistry. The spatial resolution of the CMIP5 models of atmospheric component ranges from 0.5° to 4°; however, the ocean component has spatial resolution varies from 0.2° to 2° (Taylor et al. 2012). The historical runs of CMIP5 model simulations are underestimating (overestimating) the SSTs in the Northern (Southern) Hemisphere (Wang et al. 2014). Sabeerali et al. (2013) evaluated the simulations of the BSISO over the Asian summer monsoon (ASM) region using 32 historical runs of the CMIP5 coupled GCMs models. Their findings suggest that many of the models fail to represent the peak centers of BSISO over the ISM region. However, models such as MIROC5, GFDL-CM3, IPSL-CM5A-LR, MPI-ESM-LR, and CMCC-CM are able to capture the BSISO features. Following this study, Neena et al. (2017) assessed the 27 CMIP5 model performances on BSISO variability over the Asian monsoon region by using diagnostic metrics, and their analysis revealed that the models which better simulated meridional wind, temperature, and diabatic heating have shown a realistic representation of BSISO. A recent study by Nakano and Kikuchi (2019) recommended that the CMIP5 models with an accurate representation of lower troposphere zonal wind and air-sea coupling are crucial for simulating the ISO seasonality.

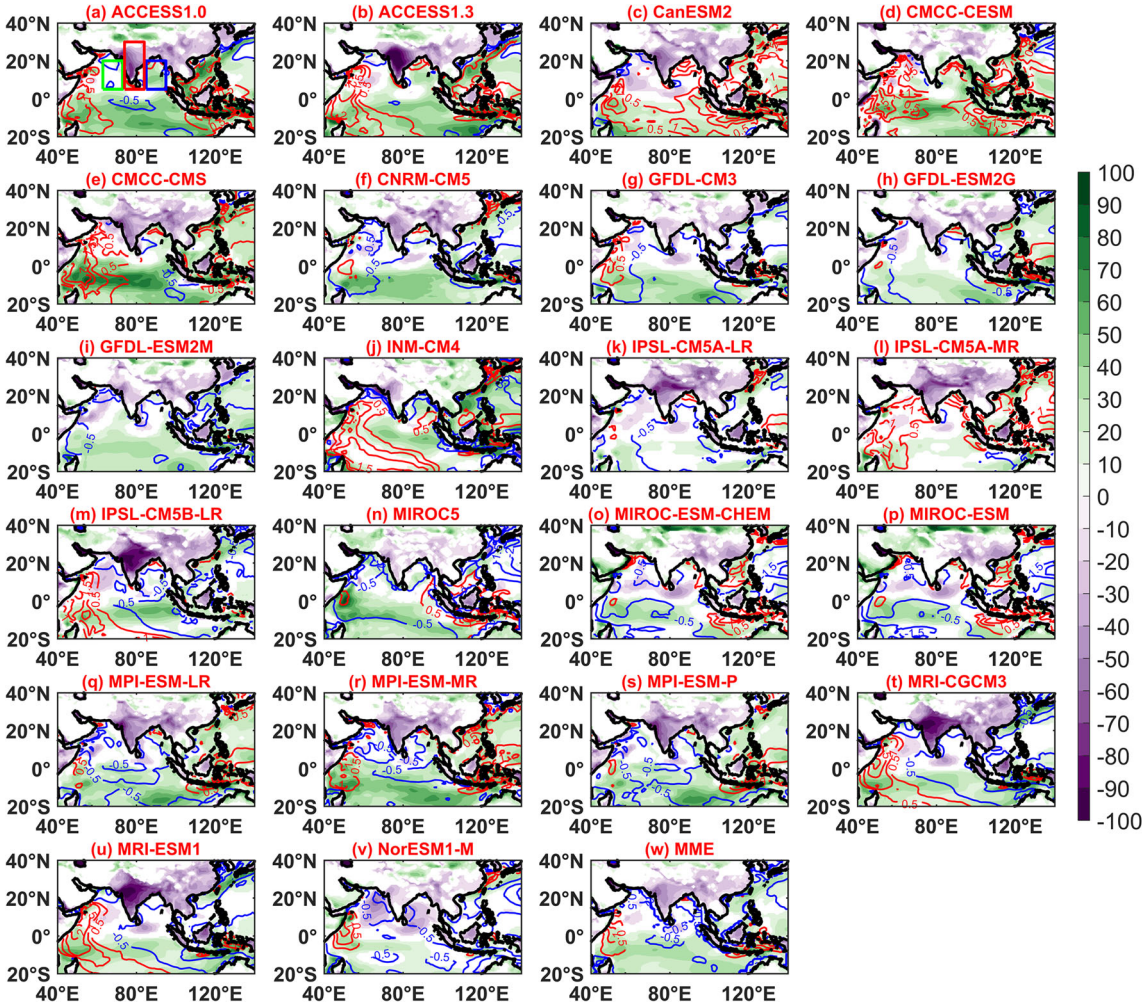

Fig. 1 The 22 CMIP5 models and MME biases (model-observations) for ISM (JJAS) seasonal mean LHF (shaded; Wm^{-2}) and SST (contours; ^{o}C; Warm biases are represented in red and cold biases are represented in blue contours). Statistically significant (0.05 significance level using t-test) regions are plotted. Insignificant values are masked with white colour. The rectangles in (**a**) represents AS (green; 63°E - 73°E, 5°N - 20°N), BoB (blue; 85°E - 95°E, 5°N - 20°N), and SCI (red; 74°E - 84°E, 5°N - 30°N)

Present study examines the performance of historical runs of CMIP5 models in representing the northward propagation of BSISO and the phase relationship between the SST, precipitation, zonal wind at 850 hPa (U850), LHF, and net heat flux (Qnet) over the NIO, AS, BoB and subcontinent of India (SCI) on ISO time scales. Main rationale and objective of the present study is to evaluate the role of local air-sea interactions for the propagation and amplitude of BSISO. The percentages of precipitation and LHF variances on ISO timescales (20–100) are shown in Fig. S1. The precipitation and LHF variances clearly show large differences between AS and BoB, however, less variance percentages differences are observed over AS and SCI. In addition, study identifies the better performance of the models of mentioned regions and its multimodel ensemble mean (MME) are presented. The remainder of the paper is organized as follows. In section 2, details of the data used and the methods are discussed. The results are presented in section 3 and cover the following aspects: the climatological features, lead-lag regression and cross-correlation analysis of air-sea fluxes. The results of MME are shown in section 4. The major conclusions and essential findings of the study are summarized in section 5.

2 Data and Methodology

We analyzed the daily precipitation, LHF, Qnet, SST, downward surface solar radiation (DSSR), U850 of 22 CMIP5 models during the period of 1980–2005. The CMIP5 models data obtained from the Program for Climate Model Diagnostic and Intercomparison (PCDMI) (https://esgf-node.llnl.gov/search/cmip5/). Models are chosen based on the availability of data. The historical runs of CMIP5 models are forced with

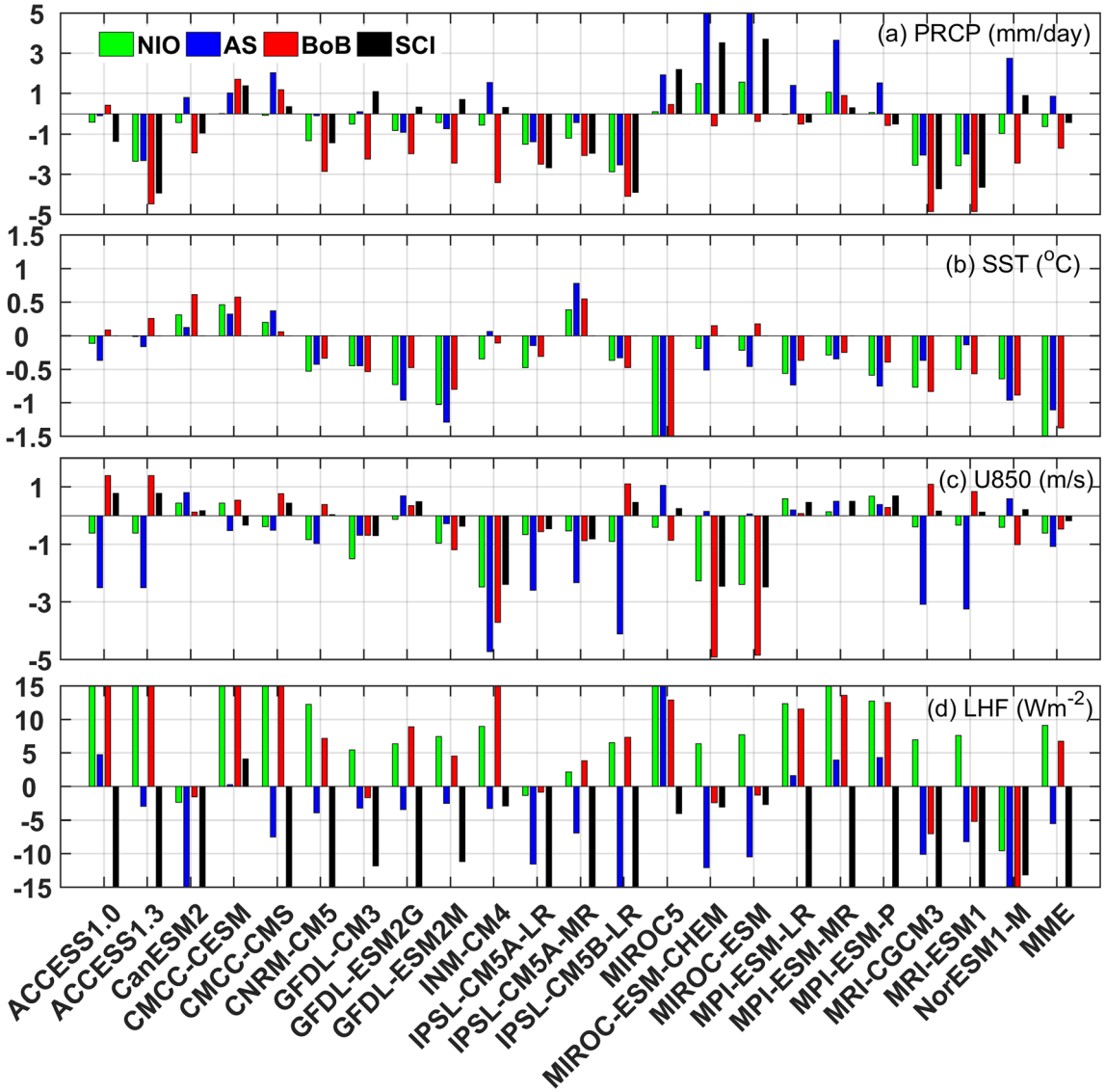

Fig. 2 The area averaged seasonal mean biases of 22 CMIP5 models and MME over NIO (60°E - 100°E, Equator - 30°N), AS (63°E - 73°E, 5°N - 20°N), BoB (85°E - 95°E, 5°N - 20°N), and SCI (74°E - 84°E, 5°N - 30°N). **a** Precipitation, **b** SST, **c** U850, and **d** LHF

natural and anthropogenic forcing to simulate the climate for the period 1850 to 2005 (Taylor et al. 2012). The names and abbreviations of 22 CMIP5 models used in this study are presented in Table 1. For each model, only one member ("r1i1p1") run is used in this study. To validate the model outputs, the daily Global Precipitation Climatology Project (GPCP) precipitation data for the period 1997 to 2005 (Huffman et al. 2001), pentad Climate Prediction Center Merged Analysis of Precipitation (CMAP) data for the period 1980 to 2005 (Xie and Arkin 1997) and Tropical Rainfall Measuring Mission (TRMM) satellite rainfall data for the period 1998 to 2005 are used. Daily DSSR, U850 are obtained from NCEP/National Center for Atmospheric Research (NCAR) Reanalysis 1, for the study period available at 2.5° × 2.5° (Kalnay et al. 1996). National Oceanic and Atmospheric Administration (NOAA) Optimum Interpolated (OI) SST data available from 1981 to 2005 (Reynolds et al. 2007) and the 3-day running mean SST based on the TRMM Microwave Imager (TMI) data for the study period available at 0.25° spatial resolution (Huffman et al. 2010). National Aeronautics and Space Administration (NASA) released the Modern Era Retrospective-Analysis for Research and Analysis (MERRA) reanalysis in 2010 based on the Goddard Earth Observing System Data Analysis System, version 5 (GEOS-5 DAS; Rienecker et al. 2011). MERRA takes advantage of a variety of recent satellite data streams. In the present study, we use MERRA latent heat flux data for the study period available at 0.6° × 0.5°

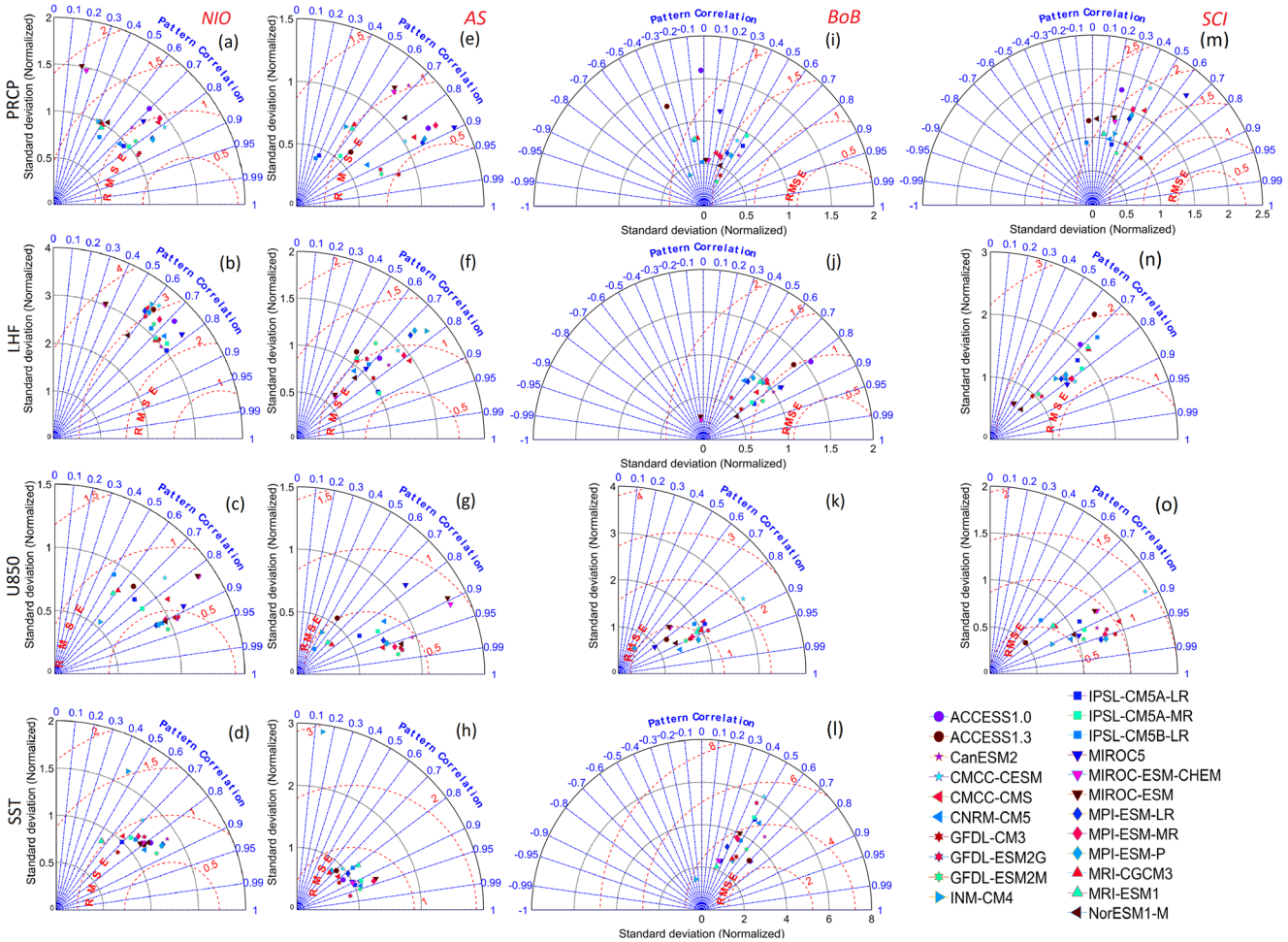

Fig. 3 Taylor diagram for the normalized pattern statistics of daily climatological JJAS means of NIO (60°E - 100°E, Equator - 30°N), AS (63°E - 73°E, 5°N - 20°N), BoB (85°E - 95°E, 5°N - 20°N), and SCI (74°E - 84°E, 5°N - 30°N). (4 columns from left to right), each column represents the precipitation, LHF, U850, and SST respectively

resolution. In the present study, observational and reanalysis products are used till 2005 only in order to assess the performance of historical runs of the CMIP5 models. All the CMIP5 model outputs, reanalysis, and observational datasets are interpolated at 1° × 1° spatial resolutions.

2.1 Methodology

The CMIP5 model's performances in representing the climatological features of ISM are assessed by using the Taylor diagram metric (Taylor 2001; Sabeerali et al. 2013, hereafter S13). This Taylor diagram metric has been employed over the regions of AS (63°E - 73°E, 5°N - 20°N), BoB (85°E - 95°E, 5°N - 20°N), NIO (60°E - 100°E, Equator - 30°N) (continental regions are masked for NIO), and SCI (74°E - 84°E, 5°N - 30°N) (Fig. 1a). These four regions are the major rainfall representative regions of the ISM (Goswami et al. 2014). The effect from atmosphere to ocean and ocean to atmosphere regulates the co-variability between the air-sea variables is similar over the AS, BoB and the SCI, different lead-lag relationships are observed over these regions (Vecchi and Harrison 2002; Roxy and Tanimoto 2007, 2012). Understanding the ocean–atmosphere processes in regulating the time response and intensity of the air-sea interactions is crucial for evaluating and rectifying (coupled) model forecasts (Wu et al. 2006; Roxy and Tanimoto 2007, 2012; DeMott et al. 2011; DeMott et al. 2014; Gao et al. 2019; DeMott et al. 2019). The daily anomalies of precipitation, SST, LHF, DSSR, and U850 are calculated from the daily climatological means (sum of annual mean and the first three harmonics). To obtain the intraseasonal variability, a 20–100 day Lanczos bandpass filter (Duchon 1979 and S13) is applied to the daily anomalies. The northward propagation of precipitation, SST, LHF, DSSR, and U850 of different models are examined using the lead-lag regression analysis. The 20–100 day bandpass filtered precipitation anomalies averaged

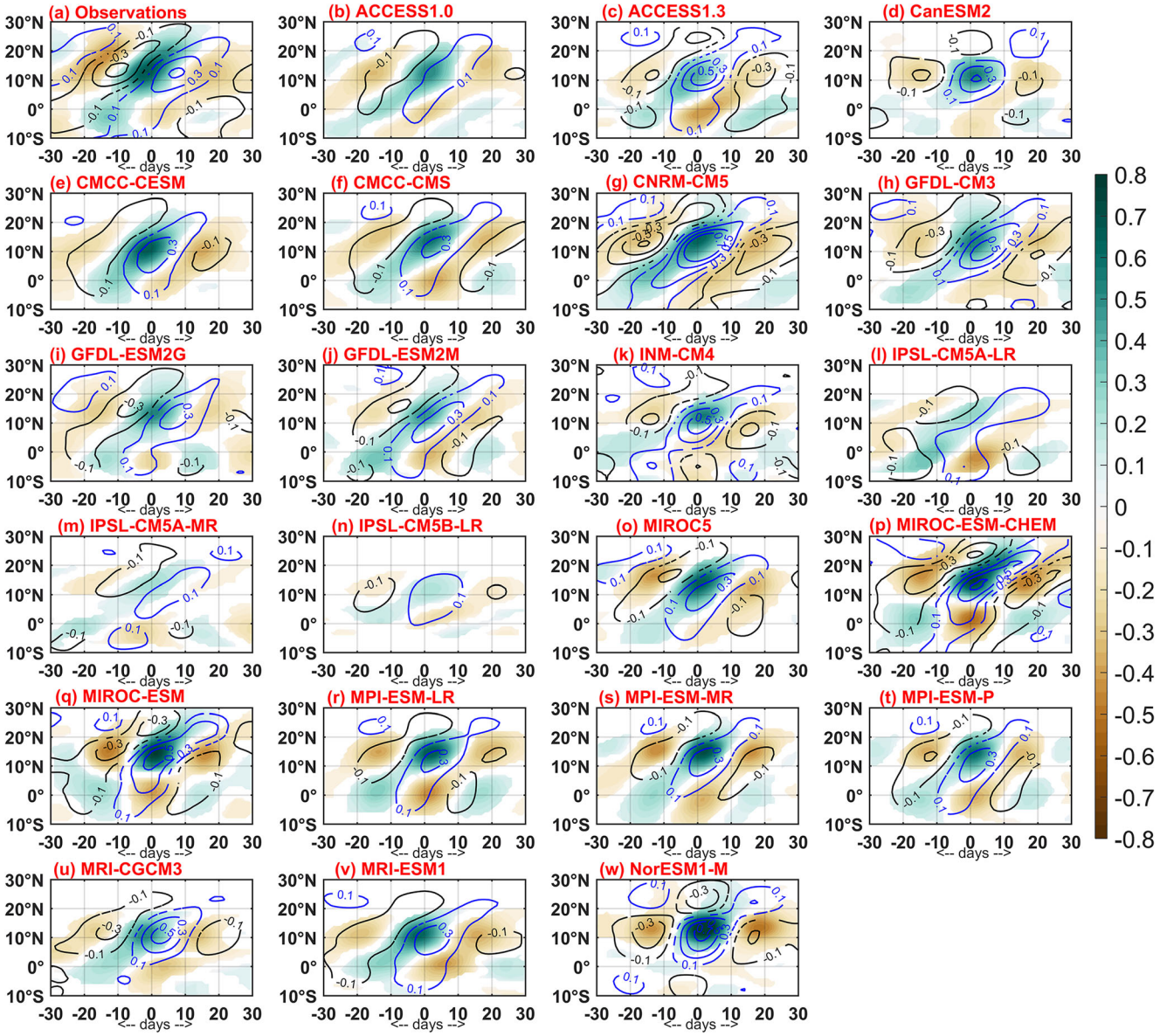

Fig. 4 Lag-latitude plot of regressed filtered precipitation anomalies (shaded; mm/day) and 850 hPa zonal wind anomalies (positive in blue and negative in black contours; m/s) averaged over the longitudes of AS (63°E - 73°E, 10°S - 30°N) illustrating the northward propagation in observations (**a**) and 22 CMIP5 models (**b** to **w**). The 20–100 day bandpass filtered precipitation anomalies averaged over the region (70°E - 90°E, 12°N - 22°N) is used as a reference time series for regression. Statistically significant (0.05 significance level using t-test) values are plotted. Insignificant values are masked with white colour

over the monsoon core region (70°E - 90°E, 12°N - 22°N) is used as a reference time-series for regression analysis, where the precipitation variance is large. On intraseasonal timescales, the phase relationship between the ocean and atmosphere interactions of different models are delineated by using the lead-lag cross-correlation analysis over the AS, BoB, NIO, and SCI. Accumulated biases are calculated as follows.

$$\text{Accumulated bias} = \sum_{i,j}^{n} |(MD(i,j) - OB(i,j))|$$

Where, i, j represents the longitude, latitude (grid points) respectively, n represents the number of grid points, MD and OB represents the regressed anomalies of the models and observations. Further, northward propagation of BSISO are identified using the recently developed metric by Ahn et al. (2020), over 0–30 lag days for positive and all regressed values. Results presented in this study are statistically significant at 95% confidence level (p values are less than 0.05 using t-test).

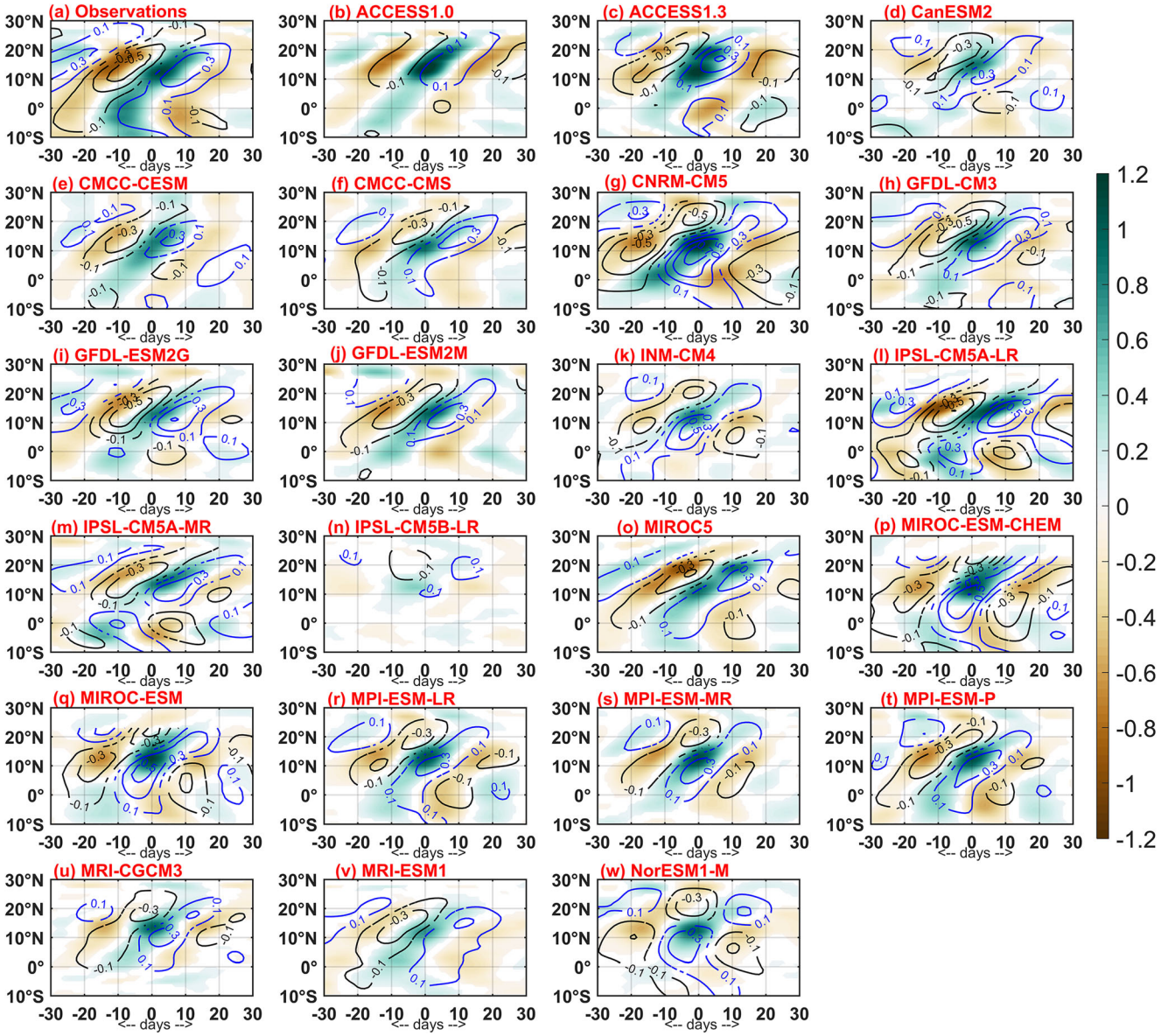

Fig. 5 Same as Fig.4 but for BoB (85°E - 95°E, 10°S - 30°N)

3 Results and Discussion

3.1 Climatological Means

The performance of 22 CMIP5 models in representing the mean characteristics of ISM precipitation, SST, LHF, and U850 are evaluated with the observations. The better representation of the BSISO associated with the ASM in a model depends on how well the model simulated the seasonal mean precipitation over the Indo-Pacific domain, and the spatial pattern of BSISO variance closely follows the spatial pattern of maximum seasonal mean precipitation regions (Ajayamohan and Goswami 2007; Sperber and Annamalai 2008; S13; Klingaman and Demott 2020). Therefore, in the present analysis we examine the ability of the models in simulating the climatological JJAS mean precipitation and air-sea fluxes. The biases of climatological means of LHF and SST of 22 CMIP5 models and MME are shown in Fig. 1. Most of the models underestimate (overestimate) the LHF over the Indian continent (Ocean region). However, the majority of models overestimate the SST over West Indian Ocean (WIO) (Fig. 1). Recent studies suggest that improper representation of oceanic currents in the WIO induced by weaker monsoon circulation are attributing the warmer SST biases in this region (Li et al. 2016; Sayantani and Gnanaseelan 2015; Fathrio et al. 2017). Moreover, the inadequate ocean dynamical cooling and LHF

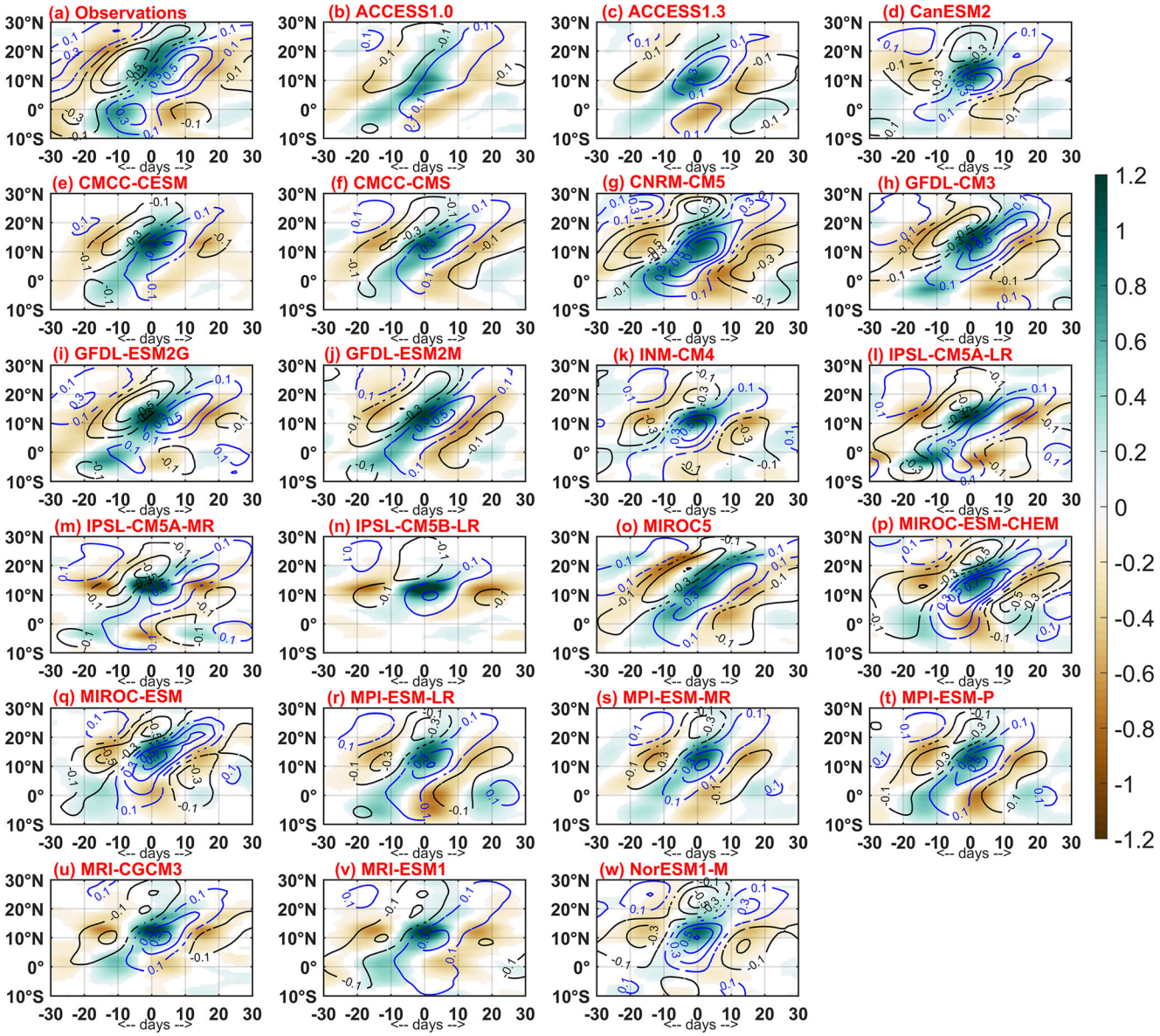

Fig. 6 Same as Fig.4 but for SCI (74°E - 84°E, 10°S - 30°N)

both are responsible for the development of warm SST biases (Yang et al. 2015). The MME (Fig. 1w) also show the underestimation of LHF over Indian region and warm SST biases over the WIO. Similarly, ISM mean precipitation biases of models are shown in Fig. S2. Most of the models are showing dry biases in the southern equatorial Indian Ocean (SEIO), SCI and BoB; however, wet biases over the Himalayan region, maritime-continent and western AS. It was found that MME (Fig. S2w) shows the excess precipitation over WIO and Himalayan region compared to the observations during the summer monsoon season. The area-averaged biases of precipitation, SST, U850, and LHF of different models over NIO, AS, BoB, and SCI (except SST) are shown in Fig. 2. The precipitation biases (Fig. 2a) is low in the models such as ACCESS1.0, CanESM2, CMCC and GFDL group of models, MPI-ESM-LR, and MPI-ESM-P. The MIROC group of models are overestimating the precipitation over all the regions. MME shows the low precipitation biases over the regions; these results are consistent with the Sperber et al. (2013). The ACCESS1.3, IPSL, and MRI group of models are underestimating the precipitation over all the regions.

To quantify the model's skill in representing the spatial pattern climatological (JJAS) mean of precipitation, LHF, U850, and SST are assessed objectively by the Taylor diagram over the regions of NIO, AS, BoB, and SCI (Fig. 3). The

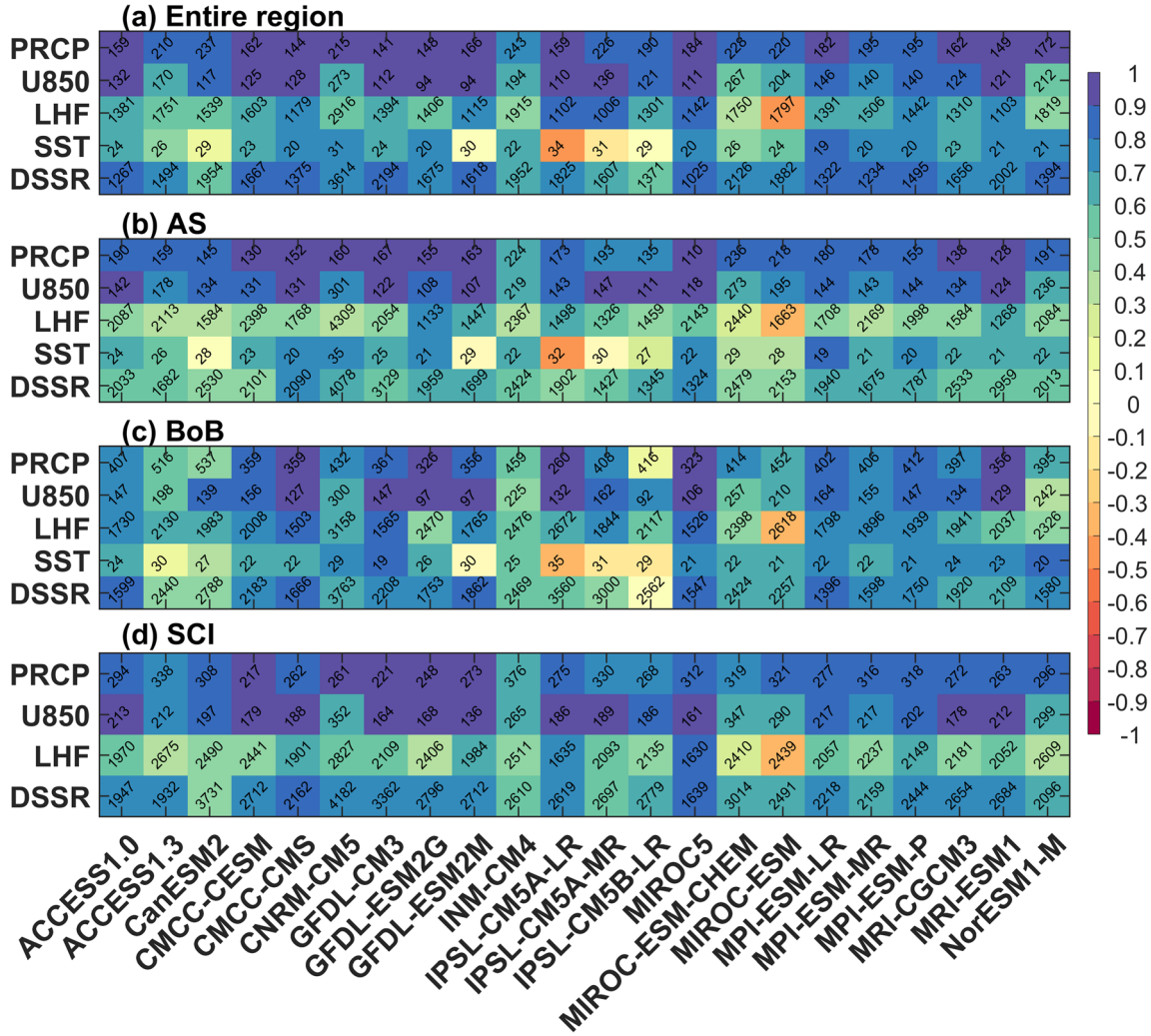

Fig. 7 Pattern correlation coefficients between 22 CMIP5 models and observations in simulating the northward propagating anomalies of precipitation, U850, LHF, SST and DSSR over entire region (60°E - 100°E, 10°S - 30°N), AS (63°E - 73°E, 10°S - 30°N), BoB (85°E - 95°E, 10°S - 30°N), and SCI (74°E - 84°E, 10°S - 30°N), respectively. Values represent the accumulated biases between models and observations

performance of the models is evaluated based on the following criterion i.e. correlation >0.7, normalized standard deviation from 0.5 to 1.5, and root mean square error < 1 (S13). Over the AS most of the models are showing of good spatial correlations precipitation, except INM-CM4, IPSL-CM5A-LR, IPSL-CM5B-LR, MRI-CGCM3, and MRI-ESM1. Over the BoB, none of the models is able to meet the specified criteria as mentioned above; however, over the SCI, the GFDL-CM3 model shows better simulation. Over the BoB in concurrence with the precipitation, most of the models show the weak SST correlation. However, most of the models show good correlations of LHF and U850 over all the regions.

3.2 Intraseasonal Propagations

The northward propagation of BSISO is evaluated in the observations, and 22 CMIP5 models using 20–100 day bandpass filtered anomalies of precipitation and U850 over AS are shown in Fig. 4. Over the AS, observations (Fig. 4a) indicate the pronounced northward propagation of precipitation and U850 anomalies from the equatorial region to the 30°N; however, a weak southward propagation of precipitation anomalies also evident. Observations (Fig. 4a) reveals that on intraseasonal timescales, maximum convection leads the westerly wind by about 7 to 8 days, which are in agreement with the findings of Hoyos and Webster (2007), Konda and Vissa (2019). Most of the CMIP5 models show the northward propagation of convection, and better propagations are shown in CMCC-CMS, CNRM-CM5, GFDL-CM3, and GFDL-ESM-2G models. MIROC5, MPI and MRI group of models show deficiency in capturing the northward propagation beyond 20°N. However, poor representation seen in INM-CM4 and IPSL group of models, and most of the models show weak or enhanced BSISO amplitudes as compared with the

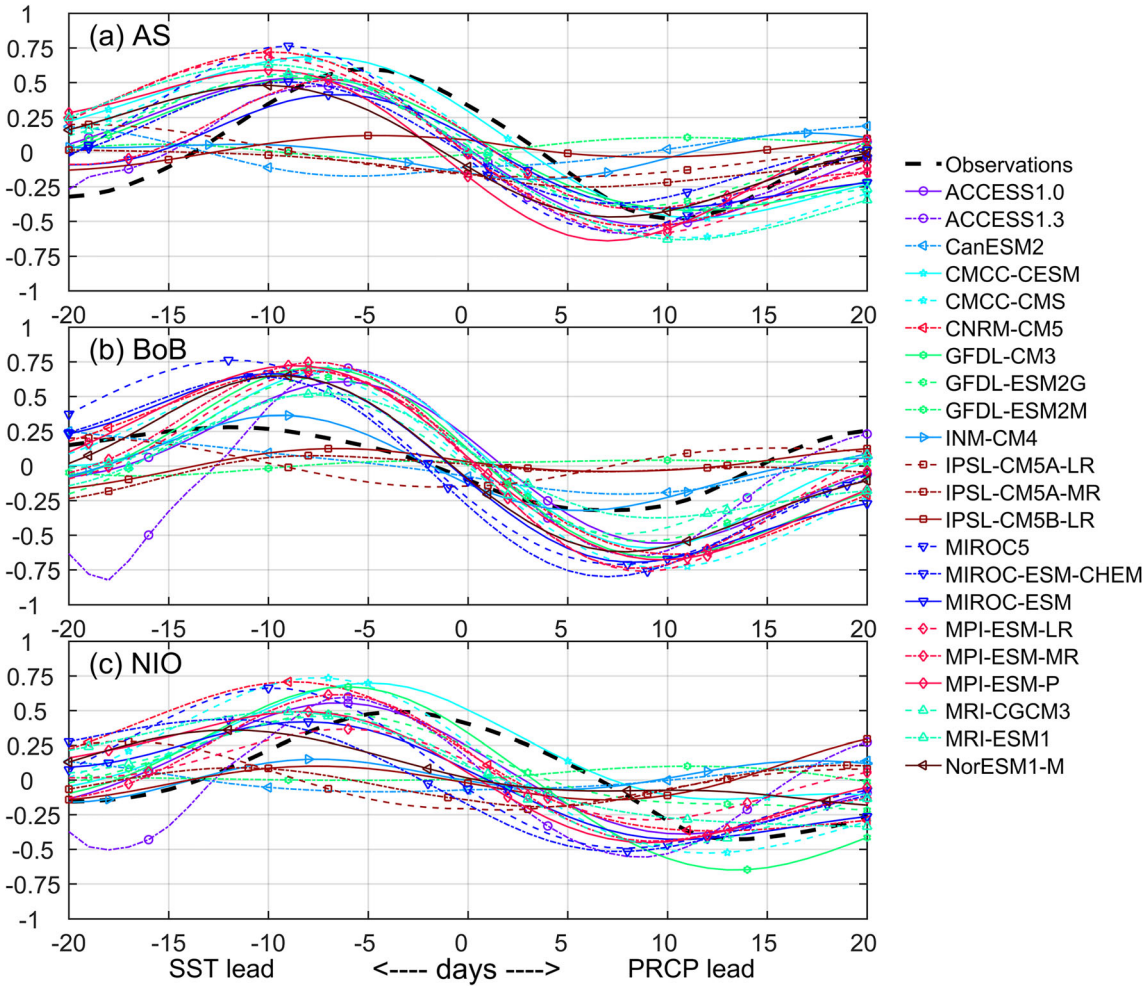

Fig. 8 Lead-lag cross-correlations of 20–100 day bandpass filtered SST and precipitation anomalies averaged over AS (63°E - 73°E, 5°N - 20°N; **a**, BoB (85°E - 95°E, 5°N - 20°N; **b**, and NIO (60°E - 100°E, Equator - 30°N; **c**. Negative (Positive) days indicate SST (precipitation) lead. Correlation values are statistically significant (0.05 significance level using t-test)

observations. The northward propagation of precipitation and U850 over BoB is shown in Fig. 5; observations (Fig. 5a) indicate that the robust northward propagation of precipitation at 10°N - 20°N with a westerly wind lags about a week. In the models, the northward propagation of precipitation and U850 over the BoB is captured by few models, e.g. CMCC-CMS, GFDL group of models, MIROC5, and IPSL-CM5A-LR. However, these models show wet biases. The models, such as IPSL-CM5B-LR and CanESM2 show large uncertainty to represent the BSISO characteristics over the BoB. Similarly, the northward propagation of BSISO over SCI is shown in Fig. 6. The northward propagation of precipitation (U850) is well captured by GFDL-CM3 (MIROC5); however, poor representation of precipitation and U850 are seen in INM-CM4 and IPSL-5B-LR models. Most of the models produce insufficient amplitude to capture the northward propagation of convection beyond 20°N. The northward propagation of precipitation and U850 for the longitudes 60°E - 100°E is shown in Fig. S3. Most of the models show the strong (weak) northward (southward) propagation of convection and its associated U850 anomalies from the Equator. The pattern correlations and their associated accumulated biases of precipitation, U850, LHF, SST, and DSSR over the entire region, AS, BoB, and SCI shown in Fig. 7. Over AS (BoB), the GFDL-ESM-2G (CMCC-CMS) model performing well in representing the northward propagation. However, IPSL group of models show negative SST correlation and large biases; similarly the IPSL group of models show weak northward migration over the South Asian high region (Shang et al. 2019). Among all the models, ACCESS1.3, INM-CM4, and MIROC-ESM-CHEM models underestimate the U850 among all the regions, which is also evident in the LHF pattern. Similarly, the GFDL-CM3 (INM-CM4) performing better (poor) over SCI. The MIROC5 model reasonably represents the northward propagation of all variables across the regions; these findings are in

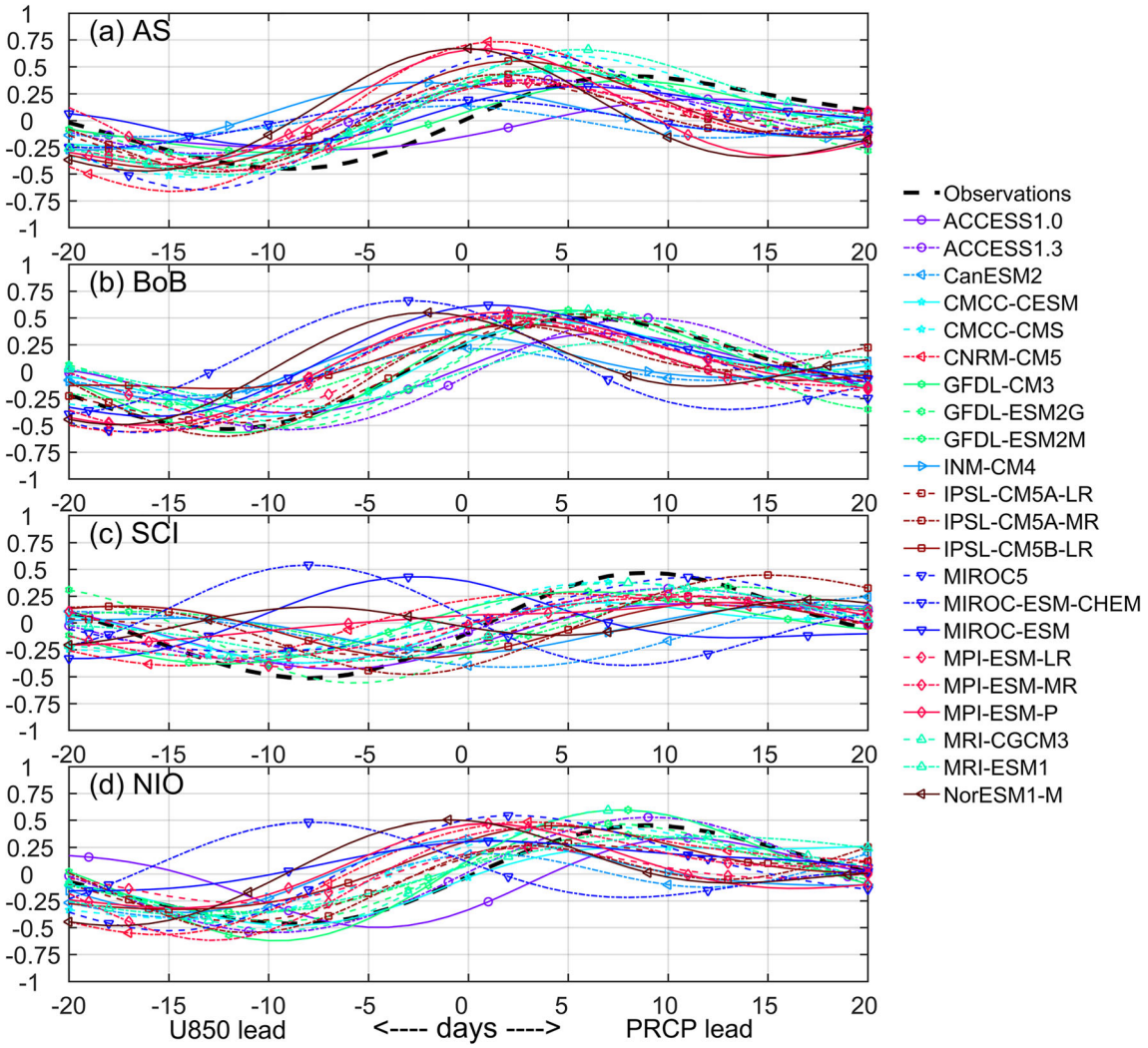

Fig. 9 Lead-lag cross-correlations of 20–100 day bandpass filtered U850 and precipitation anomalies averaged over AS (63°E - 73°E, 5°N - 20°N; **a**, BoB (85°E - 95°E, 5°N - 20°N; **b**, SCI (74°E - 84°E, 5°N - 30°N; **c**, and NIO (60°E - 100°E, Equator - 30°N; **d**. Negative (Positive) days indicate U850 (precipitation) lead. Correlation values are statistically significant (0.05 significance level using t-test)

agreement with S13. Standardized metric (Fig. S4) to identify the good/poor models in representing the northward propagating BSISO is developed (Ahn et al. 2020) for AS, BoB, and SCI.

3.3 Air-Sea Interactions

It is essential to understand the performance of models in representing the phase relationship of the ocean and atmosphere interactions (e.g. Roxy and Tanimoto 2007; Roxy et al. 2013; Sharmila et al. 2014a; Hu and Li 2017). To identify the CMIP5 models in the robust representation of ISO features of ISM over AS, BoB, SCI, and NIO we have performed lead-lag cross-correlation analysis for key diagnostic parameters such as precipitation, SST, U850, LHF, Qnet, and DSSR. The magnitude of correlation refers to the pronounced ocean-atmosphere interaction, and the corresponding lead/lag represents the response between them on ISO timescales. The phase-relationship between the parameters will vary from year to year, to avoid the discrepancy, lag-correlation performed among the seasons individually. The phase relationship between SST and precipitation over AS, BoB and NIO regions of observations and CMIP5 models are shown in Fig. 8. Over the AS (BoB) SST leads the precipitation by a 5 (12) days in the observations, which signifies the fast (slow) response from ocean to atmosphere over the AS (BoB) (Fig. 8a and b), findings are consistent with the earlier works (e.g. Sengupta et al. 2001; Roxy et al. 2013). The difference in SST-precipitation phase relationship over the AS and BoB are attributed from the meridional gradient of SST, cloud cover, phase speed, propagations of ISO, and oceanic mixed layer depth (Duvel et al. 2004; Roxy et al. 2013). Over the AS and NIO (BoB)

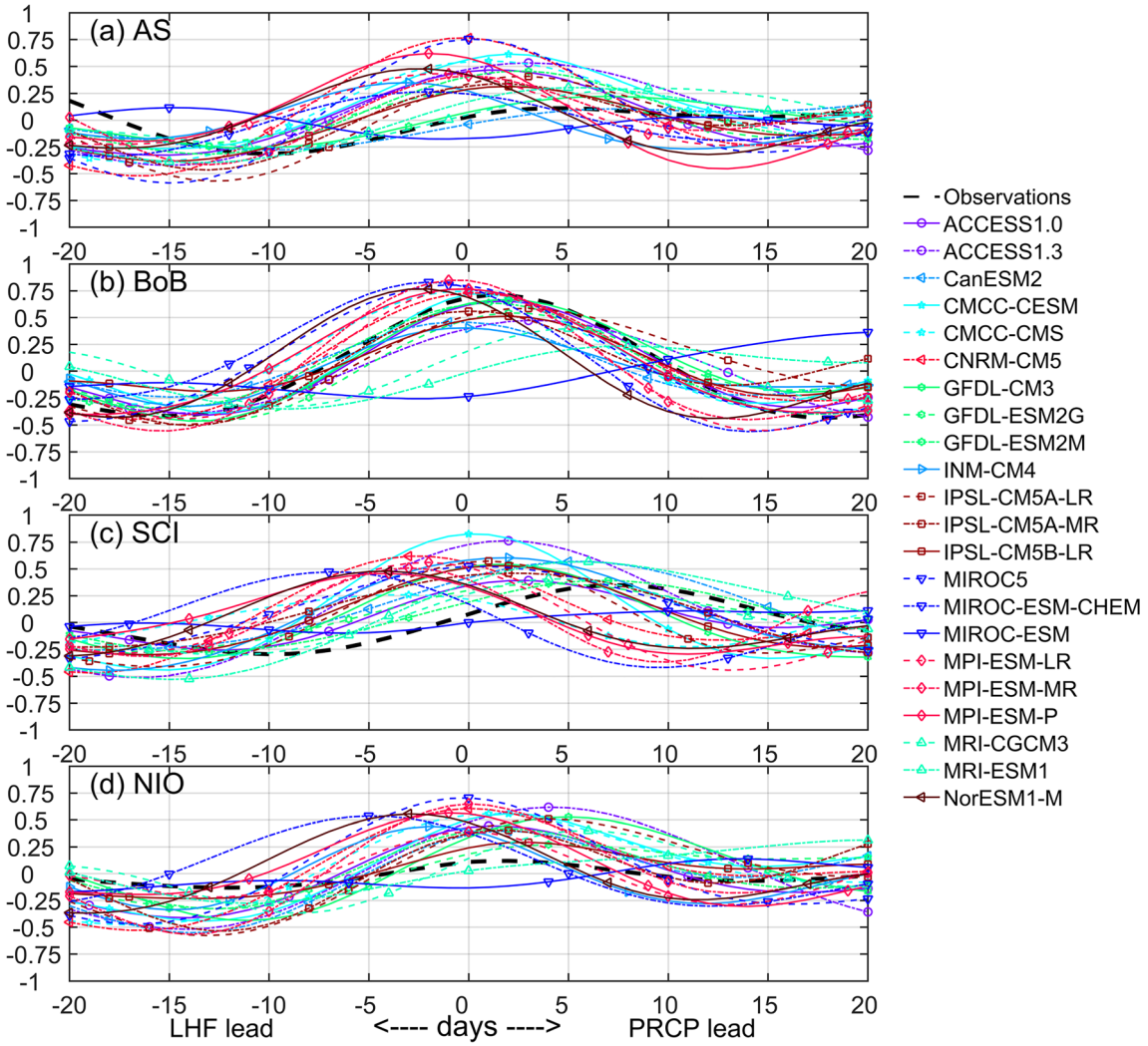

Fig. 10 Lead-lag cross-correlations of 20–100 day bandpass filtered LHF and precipitation anomalies averaged over AS (63°E - 73°E, 5°N - 20°N; **a**, BoB (85°E - 95°E, 5°N - 20°N; **b**, SCI (74°E - 84°E, 5°N - 30°N; **c**, and NIO (60°E - 100°E, Equator - 30°N; **d**. Negative (Positive) days indicate LHF (precipitation) lead. Correlation values are statistically significant (0.05 significance level using t-test)

most of the models represent the slow (fast) response from atmosphere to ocean; however, ACCESS1.3 (INM-CM4) shows the realistic representation.

The lead-lag relationship between the U850 and precipitation on ISO timescales over AS, BoB, NIO and SCI from observations and models are shown in Fig. 9. Observations reveal that westerly wind lags the peak precipitation by 8, 6, 9, and 9 days over the AS, BoB, NIO and SCI respectively; however, significant correlation (0.5) is relatively stronger over BoB. Over the oceanic regions, the GFDL-CM3 model simulates the realistic response between U850 and precipitation, whereas, over the SCI, MIROC5 shown the better phase relationship. MIROC-ESM and MIROC-ESM-CHEM models are unable to capture the U850 and precipitation lead-lag phase relationship over BoB, SCI and NIO; this could be due to the representation of convection triggering scheme and the large-scale circulations in the models (Pathak et al. 2019). Similar to the former, the relationship between the LHF and precipitation filtered anomalies in observations revealed that peak correlation about 0.72 (0.4) is found over BoB (SCI) with LHF lags the precipitation by 1 (7) day, whereas, over the AS correlation is not significant (Fig. 10). The CMCC-CESM (GFDL-ESM-2 M) model shows the representative phase relationship over the BoB (SCI); however, MIROC-ESM model insufficient to capture the phase relationship between the LHF and precipitation. The out-phase relationship between LHF and precipitation is due to the underestimation of monsoonal circulation over SCI, BoB and NIO (Huang et al. 2019). The lead-lag phase relationship between Qnet and precipitation is analyzed (Fig. 11). Over AS (BoB), Qnet leads (positive correlation) precipitation by 2 (15) days in the observations. The quick (slow) response of AS (BoB) is mainly due to the strong

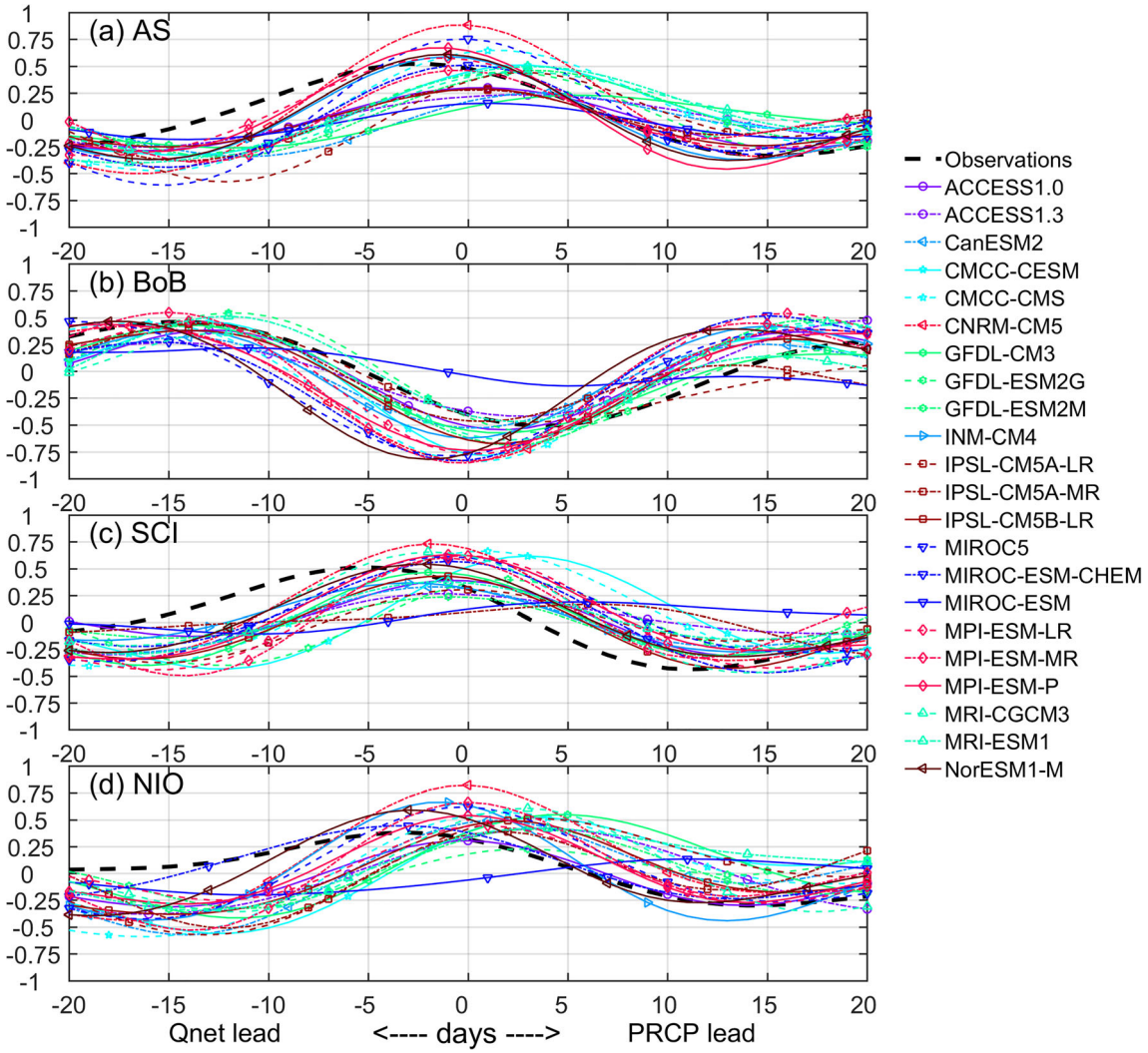

Fig. 11 Lead-lag cross-correlations of 20–100 day bandpass filtered Qnet and precipitation anomalies averaged over AS (63°E - 73°E, 5°N - 20°N; **a**, BoB (85°E - 95°E, 5°N - 20°N; **b**, SCI (74°E - 84°E, 5°N - 30°N; **c**, and NIO (60°E - 100°E, Equator - 30°N; **d**. Negative (Positive) days indicate Qnet (precipitation) lead. Correlation values are statistically significant (0.05 significance level using t-test)

monsoonal winds and associated cloud cover over the regions, AS losses more heat than BoB; results are consistent with Pokhrel et al. (2020) and Karmakar and Misra (2020). However, over SCI Qnet leads precipitation by 5 days. The lead-lag phase relationship between the DSSR and precipitation on ISO timescales of observations and CMIP5 models are shown in Fig. 12. Over AS (BoB), DSSR leads the precipitation by 11 (16) days (Fig. 12a and b). Over the AS, most of the models show the weak phase relationship; however, over BoB (SCI) CMCC-CMS model is able to capture the DSSR-precipitation phase relationship. The lead-lag relationship between the DSSR and SST filtered anomalies over AS, BoB, and NIO are shown in Fig. 13. Over AS, BoB and NIO, DSSR leads the SST by 8, 2 and 11 days respectively. The GFDL-CM3 shows a better representation over the AS (Fig. 13a); however, CMIP5 models unable to capture the phase relationship between the DSSR and SST over BoB (Fig. 13b). The summary of lead-lag relationship and peak correlations of SST, precipitation, U850, LHF, Qnet, and DSSR over AS, BoB, NIO, and SCI of observations and 22 CMIP5 models are shown in Fig. 14. Over the AS, BoB, and NIO lead-lag phase relationship of precipitation, SST, LHF, and DSSR are consistent with the findings of earlier researchers (e.g. Shinoda et al. 1998; Woolnough et al. 2000; Sengupta et al. 2001; Hoyos and Webster 2007; Roxy et al. 2013; Hu and Li 2017). Over the BoB (AS), the lead-lag phase relationship between DSSR and SST has shown a quick (slow) response, this is attributed due to the presence of shallower (deeper) mixed layer (e.g. Thadathil et al. 2007, 2008; Vissa et al. 2013; Li et al. 2018).

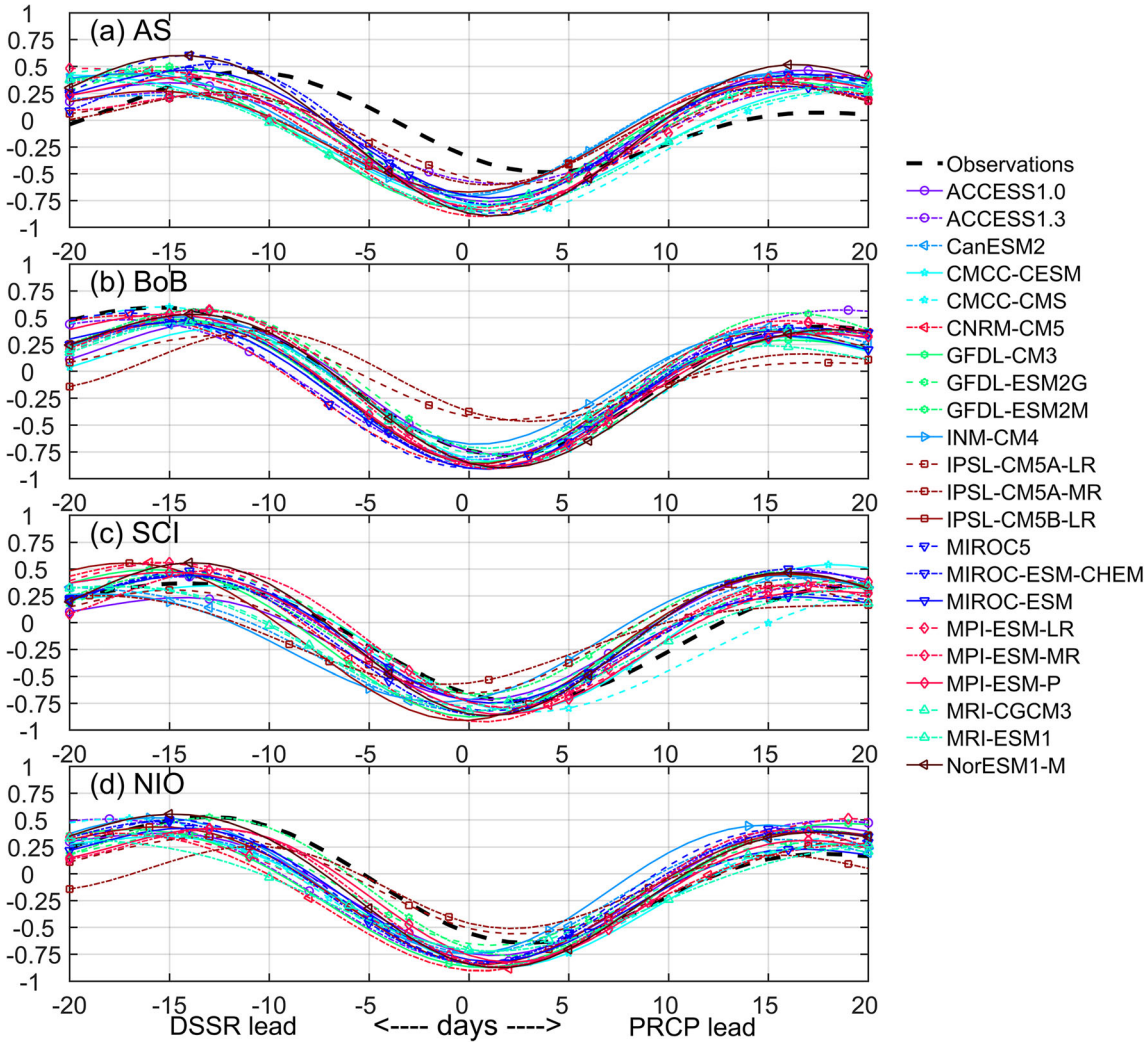

Fig. 12 Lead-lag cross-correlations of 20–100 day bandpass filtered DSSR and precipitation anomalies averaged over AS (63°E - 73°E, 5°N - 20°N; **a**, BoB (85°E - 95°E, 5°N - 20°N; **b**, SCI (74°E - 84°E, 5°N - 30°N; **c**, and NIO (60°E - 100°E, Equator - 30°N; **d**. Negative (Positive) days indicate DSSR (precipitation) lead. Correlation values are statistically significant (0.05 significance level using t-test)

4 Multi Model Ensembles

The multimodel ensemble (MME) is developed by using the arthematic mean. For MME the better models are selected over the regions of AS, BoB, SCI and NIO based upon the high pattern correlation and the better lead-lag phase relationship in consistent with the observations. Models selected for the MME over the regions are given in Table 2. The MME shows the near realistic northward propagation (both amplitude and phase) of convection and associated U850 anomalies over AS, BoB, and SCI (Fig. 15a, c, e) with observation, however, biases persists in both northward propagation and amplitude. Over the AS, MME shows the slow response of SST and precipitation (Fig. 15b). However, MME fails to represent the phase relationship between the LHF and precipitation over AS and SCI. The in-phase relationship of Qnet and precipitations is evident in MME (Fig. 15b). Over BoB, in MME the phase relationship of SST, precipitation, LHF, DSSR and U850 are consistent with the observations (Fig. 15d). Over NIO, MME shows the good agreement in phase relationship between the ocean and atmosphere interactions (Fig. 15g). The MME for poor models is given in (Fig. 16). Over AS and BoB models fail to represent the northward propagation BSISO. However, over SCI MME represents the northward propagating BSISO (Fig. 16e). Over AS MME shows the in-phase relationship of DSSR and SST (Fig. 16b). MME also resemble the DSSR and PRCP relationship over BoB (Fig. 16d).

5 Conclusions

The ISM displays strong ISV, manifest as northward propagating convection anomalies from the equatorial Indian Ocean to the foothills of Himalayas. In the present study, the

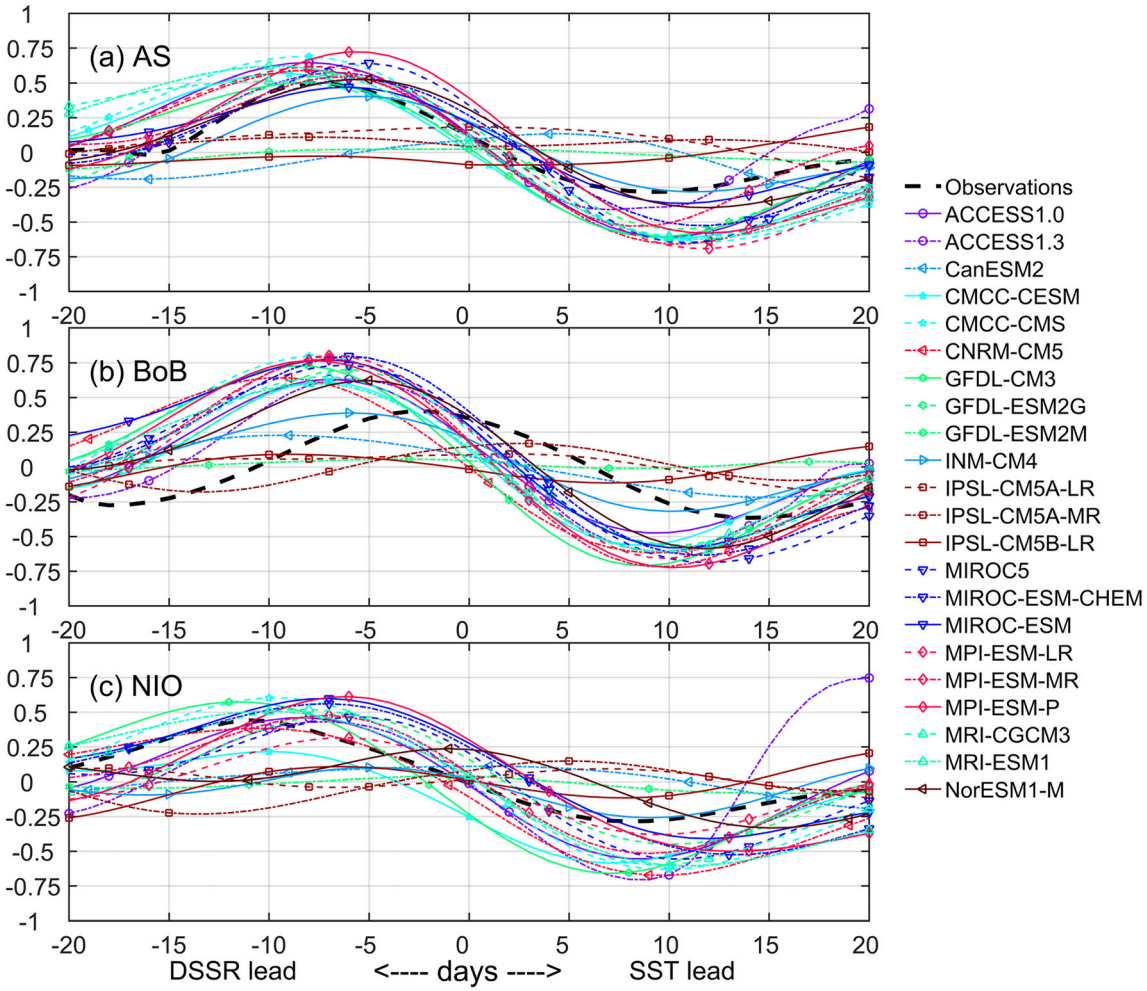

Fig. 13 Lead-lag cross-correlations of 20–100 day bandpass filtered DSSR and SST anomalies averaged over AS (63°E - 73°E, 5°N - 20°N; **a**, BoB (85°E - 95°E, 5°N - 20°N; **b**, and NIO (60°E - 100°E, Equator - 30°N; **c**. Negative (Positive) days indicate DSSR (SST) lead. Correlation values are statistically significant (0.05 significance level using t-test)

evaluation of BSISO and its associated exchange of air-sea fluxes at the air-sea interface are analyzed in the 25 (1980–2005) year climate simulations of 22 CMIP5 model outputs (historical runs) were compared with the observations. A set of evaluation metrics were developed and used to assess the representation of summer mean state, northward propagation of BSISO and its associated air-sea interactions over AS, BoB and SCI during ISM season on intraseasonal time scales. The majority of the models are underestimating the LHF over the subcontinent of India and overestimates the southern equatorial Indian Ocean. Similarly, most of the models are underestimating the precipitation over BoB, east equatorial Indian Ocean, and overestimates the precipitation over the west equatorial Indian Ocean. High dry biases are found in the MIROC group of models. Comparisons of mean state features with northward propagation of BSISO are presented in Table 3. That model which fails to simulate/underestimate the mean state can degrade the northward propagation of BSISO. Findings are consistent with the Klingaman and DeMott (2020), in coupled models large biases in mean state can degrade/inhibit the propagation of ISO.

The northward propagating BSISO plays an essential role in modulating the onset, active and break spell of the monsoon. Lead/Lag regression analysis is used to evaluate the propagation features of BSISO. Large discrepancies were observed in the models depiction of the northward propagating precipitation, U850, LHF, SST and DSSR anomalies. Over the Indian Ocean, proper representation of surface turbulent fluxes in the coupled models can simulate the realistic intraseasonal convection (DeMott et al. 2014). In the present study, the models (e.g. GFDL CM3, GFDL ESM 2G) which show represent northward propagation of air-sea fluxes and phase-relationships could simulate the BSISO reasonably.

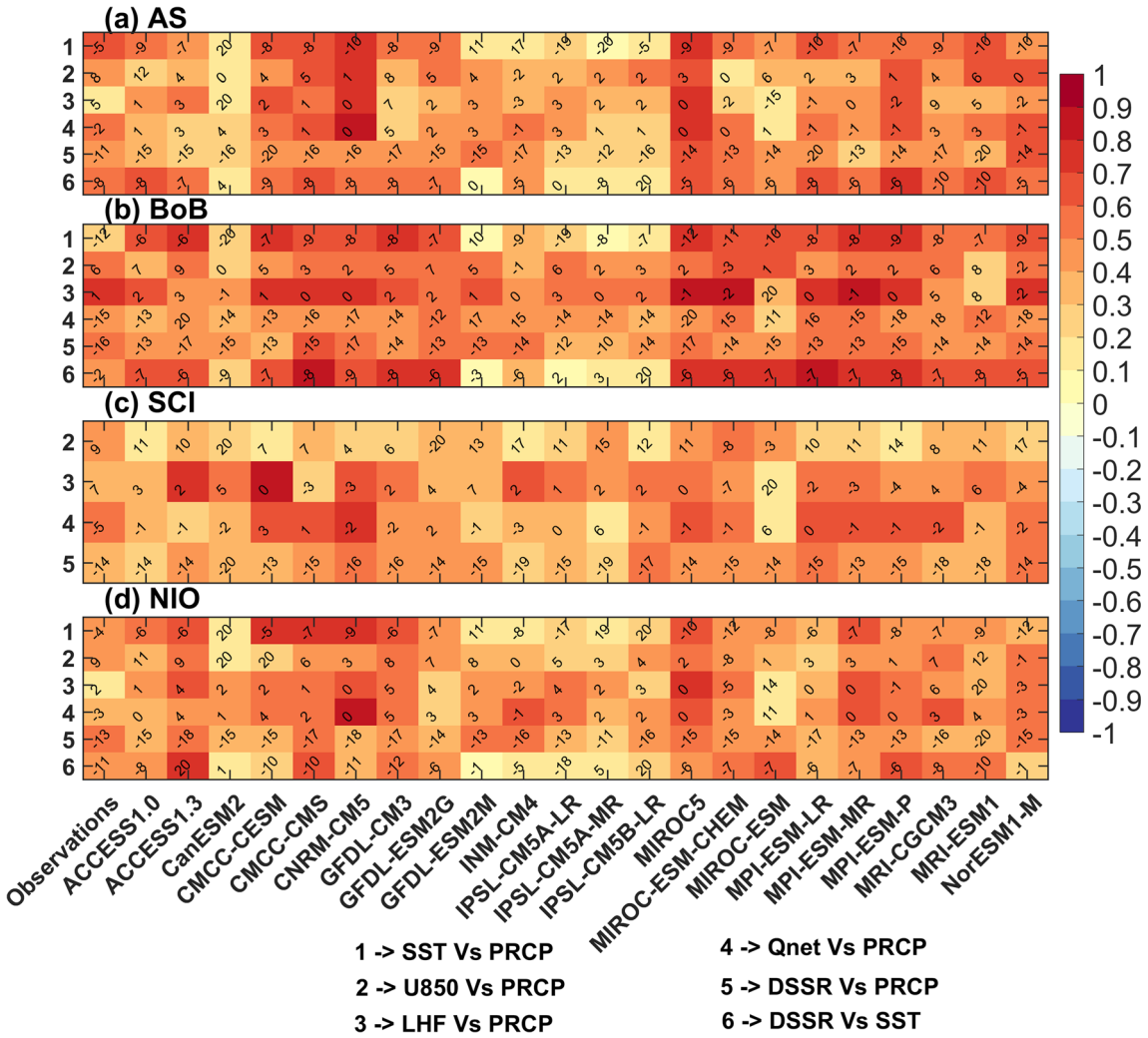

Fig. 14 Lead-lag correlation (shaded) and its associated days (numbers) for SST Vs PRCP, U850 Vs PRCP, LHF Vs PRCP, Qnet Vs PRCP, DSSR Vs PRCP and DSSR Vs SST respectively over **a** AS, **b** BoB, **c** SCI, and **d** NIO. Negative (Positive) days indicate surface fluxes (precipitation) lead

Most of the models replicate the northward propagation convection with strong biases over AS, BoB and SCI, however the majority of the models unable to represent the LHF anomalies associated with precipitation and U850 (Fig. 7). Few models (e. g. CMCC-CMS, GFDL-CM3, and MIROC5) show the realistic northward propagations over Indian regions. Most of the models produce insufficient amplitude to capture the northward propagation of convection beyond 20°N.

The performance of CMIP5 models in simulating the climatological means, northward propagation and air-sea interactions phase relationship over AS, BoB, SCI and entire region are presented in Table 3. The performance of the models is evaluated based on the following criterion i.e. pattern

Table 2 Model selected for the MME analysis over AS, BoB, SCI, and NIO. Models used for MME are good in representing of BSISO and its associated air-sea interactions

AS	BoB	SCI	NIO
CMCC-CMS	ACCESS1.3	CMCC-CMS	CMCC-CMS
CMCC-CESM	CMCC-CMS	CMCC-CESM	CMCC-CESM
GFDL-ESM-2G	GFDL-CM3	GFDL-ESM-2G	GFDL-CM3
MPI-ESM-MR	GFDL-ESM-2G	MIROC5	GFDL-ESM-2G
MPI-ESM-P	MPI-ESM-P	MPI-ESM-LR	
	MIROC5		

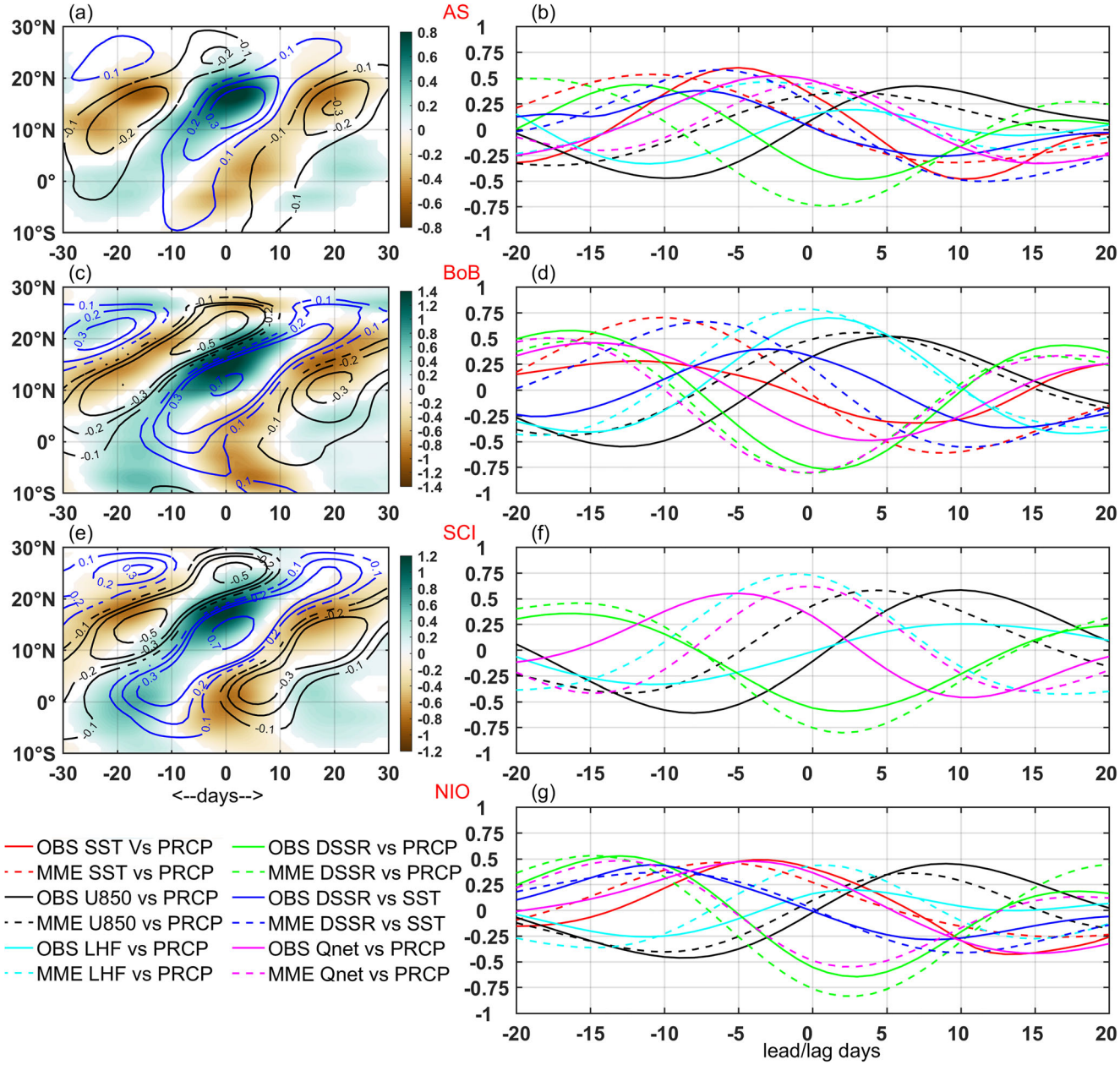

Fig. 15 MME lag-latitude (left panel) regressed filtered precipitation anomalies (shaded; mm/day) and 850 hPa zonal wind anomalies (positive in blue and negative in black contours; m/s) over AS (63°E - 73°E, 10°S - 30°N; **a**, BoB (85°E - 95°E, 10°S - 30°N; **c**, and SCI (74°E - 84°E, 10°N - 30°N; **e**. Lead-lag cross-correlation (right panel) of MME of precipitation, SST, U850, LHF, and DSSR over AS (63°E - 73°E, 5°N - 20°N; **b**, BoB (85°E - 95°E, 5°N - 20°N; **d**, SCI (74°E - 84°E, 5°N - 30°N; **f**, and NIO (60°E - 100°E, Equator - 30°N; **g**

correlation >0.7, normalized standard deviation from 0.5 to 1.5, and root mean square error < 1 (S13). Models which represented the realistic climatological means of precipitation, SST, 850 hPa winds and, LHF are performed reasonable well for the northward propagation of convection, SST, winds and air-sea fluxes viz. CMCC-CESM, GFDL-CM3, GFDL-ESM2G and MIROC5. However, these models are insufficient to represent realistic amplitude of northward propagation, which can be attributed due to the improper phase-relationship of the air-sea interactions especially over the BoB. Findings from the present study are consistent with the observational analysis of Gao et al. (2019).

The local air-sea interactions play an essential role during intraseasonal propagation of precipitation (Woolnough et al. 2000; Sengupta et al. 2001; Zhang et al. 2018; Yang et al. 2019a, b). The point-wise Lead/Lag cross-correlation analysis has been used to analyze the representation of local air-sea relationships in the observations and 22 CMIP5 models, utilizing the air-sea variables. Significant correlations are found between SST and precipitation. This relationship shows the

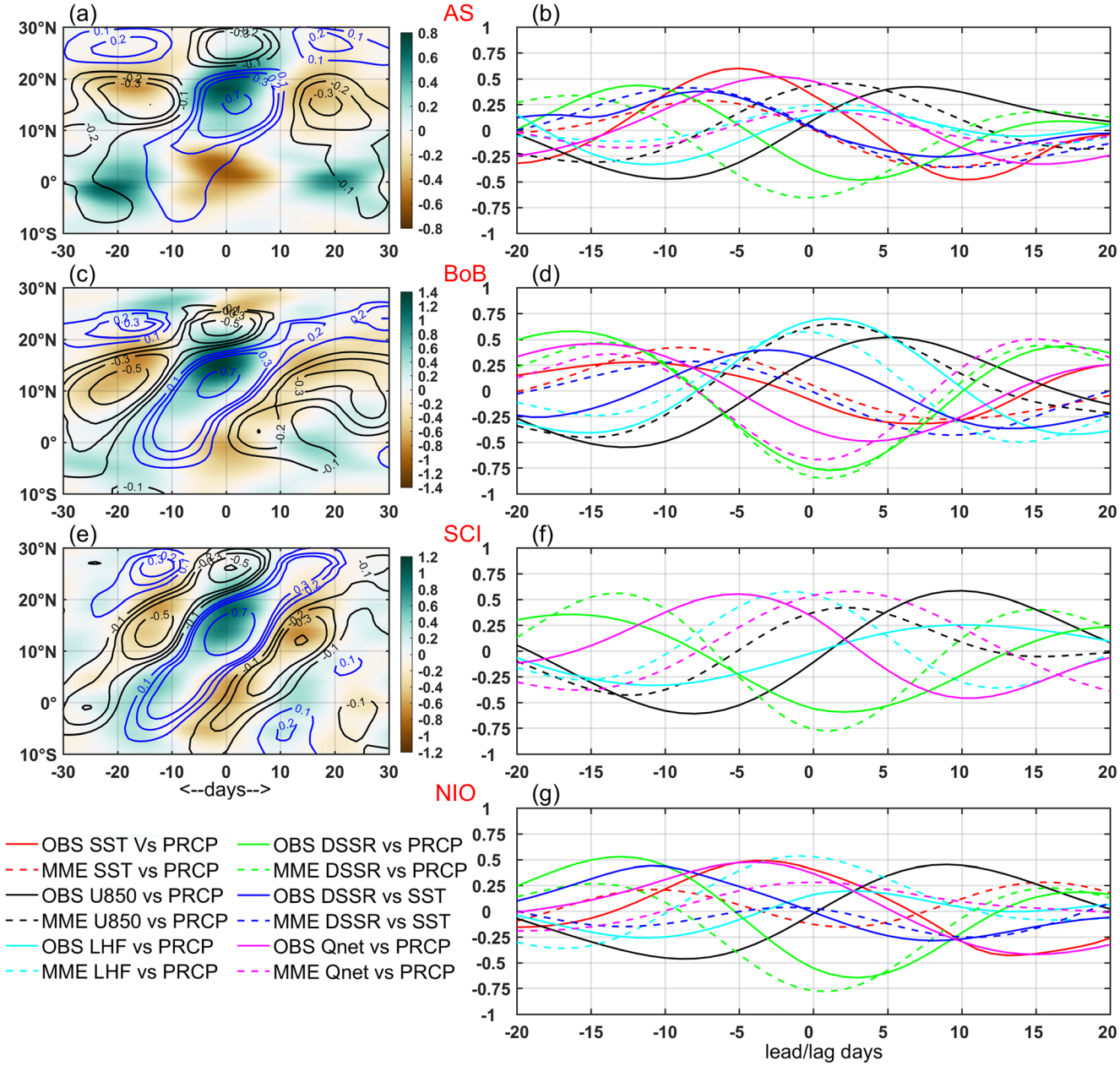

Fig. 16 Same as Fig.15 but for MME of poor models

quick (slow) response from Ocean to Atmosphere over AS (BoB) with SST leads precipitation by 5 (12) days in the observations, whereas, CMIP5 models show the slow (quick) response from Ocean to Atmosphere over AS (BoB). Similarly, significant correlations are found between SST and DSSR, when the DSSR leads SST by 8 (2) days over AS (BoB). The majority of the CMIP5 models show the slow response from Atmosphere to Ocean over the AS and BoB. By analysing the different aspects of the air-sea variable, it is found that CMCC, GFDL group of models and MIROC5 models are able to represent the air-sea interaction on intraseasonal time scales; however, MIROC-ESM model show large uncertainty representing the air-sea interactions. The MME (Fig. 15) represents the near realistic northward propagation of convection and its associated U850 anomalies over AS, BoB, and SCI. Most of the CMIP5 models resemble in-phase relationship between DSSR and PRCP. MME insufficient to represents the relation between precipitation and LHF over AS and SCI; however it shows the in-phase relationship over BoB and NIO. MME (Fig. 15) well represented the in-phase relationship of air-sea fluxes over NIO. Poor MME (PMME) lag-latitude regression and air-sea phase relationship are shown in Fig. 16; results reveal clear differences between MME and PMME. Many recent studies were identified the increase of the seasonal mean ISM rainfall in the future climate (Sharmila et al. 2014b; Lee and Wang 2014;

Table 3 Performance of CMIP5 models in simulating the climatological means, northward propagation of BSISO, and air-sea interactions over the regions

Models	JJAS mean climatological features				Northward propagation of the BSISO		Phase relationship of the BSISO				
	AS	BoB	SCI	NIO	AS	BoB	SCI	AS	BoB	SCI	NIO
ACCESS1.0	✓	✗	✗	✓	✓	✓	✓	✗	✗	✗	✓
ACCESS1.3	✓	✓	✗	✗	✗	✗	✗	✓	✓	✗	✓
CanESM2	✓	✗	✓	✓	✗	✗	✗	✗	✗	✗	✗
CMCC-CESM	✓	✗	✓	✓	✓	✓	✓	✓	✗	✓	✓
CMCC-CMS	✓	✗	✗	✗	✓	✓	✓	✓	✓	✓	✓
CNRM-CM5	✓	✗	✗	✓	✓	✗	✗	✓	✗	✗	✗
GFDL-CM3	✓	✓	✓	✓	✓	✓	✓	✓	✓	✓	✓
GFDL-ESM2G	✓	✓	✓	✓	✓	✓	✓	✓	✓	✓	✓
GFDL-ESM2M	✗	✗	✗	✓	✗	✗	✓	✗	✗	✓	✗
INM-CM4	✗	✗	✗	✗	✗	✗	✗	✗	✗	✗	✗
IPSL-CM5A-LR	✓	✓	✗	✓	✗	✗	✓	✗	✗	✗	✓
IPSL-CM5A-MR	✓	✗	✓	✗	✗	✗	✗	✗	✗	✗	✓
IPSL-CM5B-LR	✗	✗	✗	✓	✗	✗	✗	✓	✗	✗	✗
MIROC5	✓	✓	✓	✗	✓	✓	✓	✗	✓	✓	✗
MIROC-ESM-CHEM	✗	✗	✗	✗	✗	✗	✗	✗	✗	✗	✗
MIROC-ESM	✗	✗	✗	✗	✗	✗	✗	✗	✗	✗	✗
MPI-ESM-LR	✓	✗	✓	✗	✓	✓	✓	✗	✗	✓	✗
MPI-ESM-MR	✓	✗	✗	✗	✓	✓	✗	✓	✗	✗	✗
MPI-ESM-P	✓	✓	✗	✓	✓	✓	✓	✗	✓	✗	✗
\MRI-CGCM3	✗	✗	✗	✗	✗	✓	✗	✗	✗	✓	✓
MRI-ESM1	✗	✗	✗	✗	✓	✓	✓	✗	✗	✓	✗
NorESM1-M	✓	✓	✗	✗	✗	✗	✗	✗	✗	✗	✗

Jayasankar et al. 2015; Kadel et al. 2018; Yang et al. 2019a, b). The accurate representation of air-sea fluxes, Ocean and Atmospheric processes in the models is necessary to predict the future climate more realistically.

Supplementary Information The online version contains supplementary material available at https://doi.org/10.1007/s13143-021-00228-3.

Acknowledgements Authors would like to acknowledge the Science and Engineering Research Board (SERB), Government of India (Grant Ref: ECR/2016/001896). Authors would like to thank the Editor and two anonymous reviewers for their constructive comments and helpful suggestions.

References

Abhik, S., Halder, M., Mukhopadhyay, P., Jiang, X., Goswami, B.N.: A possible new mechanism for northward propagation of boreal summer intraseasonal oscillations based on TRMM and MERRA reanalysis. Clim. Dyn. **40**(7–8), 1611–1624 (2013). https://doi.org/10.1007/s00382-012-1425-x

Ahn, M.S., Kim, D., Kang, D., Lee, J., Sperber, K.R., Gleckler, P.J., Jiang, X., Ham, Y.G. and Kim, H.: MJO propagation across the maritime continent: Are CMIP6 Models Better than CMIP5 Models?. Geophys. Rese. Lett. p.e2020GL087250 (2020). https://doi.org/10.1029/2020GL087250

Ajayamohan, R.S., Goswami, B.N.: Dependence of simulation of boreal summer tropical intraseasonal oscillations on the simulation of seasonal mean. J. Atmos. Sci. **64**, 460–478 (2007). https://doi.org/10.1175/JAS3844.1

Ajayamohan, R.S., Annamalai, H., Luo, J.J., Hafner, J., Yamagata, T.: Poleward propagation of boreal summer intraseasonal oscillations in a coupled model: role of internal processes. Clim. Dyn. **37**(5–6), 851–867 (2011). https://doi.org/10.1007/s00382-010-0839-6

Anandh, P.C., Vissa, N.K., Broderick, C.: Role of MJO in modulating rainfall characteristics observed over India in all seasons utilizing TRMM. Int. J. Climatol. **38**(5), 2352–2373 (2018). https://doi.org/10.1002/joc.5339

Attada, R., Dasari, H.P., Chowdary, J.S., Yadav, R.K., Knio, O., Hoteit, I.: Surface air temperature variability over the Arabian peninsula and its links to circulation patterns. Int. J. Climatol. **39**(1), 445–464 (2019). https://doi.org/10.1002/joc.5821

Azad, S., Rajeevan, M.: Possible shift in the ENSO-Indian monsoon rainfall relationship under future global warming. Sci. Rep. **6**, 20145 (2016)

Choudhary, A., Dimri, A.P., Paeth, H.: Added value of CORDEX-SA experiments in simulating summer monsoon precipitation over India. Int. J. Climatol. **39**(4), 2156–2172 (2019)

Chowdary, J.S., Patekar, D., Srinivas, G., Gnanaseelan, C., Parekh, A.: Impact of the indo-Western Pacific Ocean capacitor mode on south Asian summer monsoon rainfall. Clim. Dyn. **1-12**, 2327–2338 (2019). https://doi.org/10.1007/s00382-019-04850-w

Danabasoglu, G., Large, W.G., Tribbia, J.J., Gent, P.R., Briegleb, B.P., McWilliams, J.C.: Diurnal coupling in the tropical oceans of CCSM3. J. Clim. **19**(11), 2347–2365 (2006). https://doi.org/10.1175/JCLI3739.1

DeMott, C.A., Stan, C., Randall, D.A., Kinter III, J.L., Khairoutdinov, M.: The Asian monsoon in the superparameterized CCSM and its relationship to tropical wave activity. J. Clim. **24**(19), 5134–5156 (2011)

DeMott, C.A., Stan, C., Randall, D.A.: Northward propagation mechanisms of the boreal summer intraseasonal oscillation in the ERA-interim and SP-CCSM. J. Clim. **26**(6), 1973–1992 (2013). https://doi.org/10.1175/JCLI-D-12-00191.1

DeMott, C.A., Stan, C., Randall, D.A., Branson, M.D.: Intraseasonal variability in coupled GCMs: the roles of ocean feedbacks and model physics. J. Clim. **27**(13), 4970–4995 (2014)

DeMott, C.A., Klingaman, N.P., Woolnough, S.J.: Atmosphere-ocean coupled processes in the madden-Julian oscillation. Rev. Geophys. **53**(4), 1099–1154 (2015)

DeMott, C.A., Klingaman, N.P., Tseng, W.L., Burt, M.A., Gao, Y., Randall, D.A.: The convection connection: how ocean feedbacks affect tropical mean moisture and MJO propagation. J. Geophys. Res.-Atmos. **124**(22), 11910–11931 (2019)

Duchon, C.E.: Lanczos filtering in one and two dimensions. J. Appl. Meteorol. **18**(8), 1016–1022 (1979)

Duvel, J.P., Roca, R., Vialard, J.: Ocean mixed layer temperature variations induced by intraseasonal convective perturbations over the Indian ocean. J. Atmos. Sci. **61**(9), 1004–1023 (2004). https://doi.org/10.1175/1520-0469(2004)061<1004:OMLTVI>2.0.CO;2

Fathrio, I., Iizuka, S., Manda, A., Kodama, Y.M., Ishida, S., Moteki, Q., Yamada, H., Tachibana, Y.: Assessment of western Indian Ocean SST bias of CMIP5 models. J. Geophys. Res. Oceans. **122**(4), 3123–2140 (2017). https://doi.org/10.1002/2016JC012443

Frolicher, T.L., Sarmiento, J.L., Paynter, D.J., Dunne, J.P., Krasting, J.P., Winton, M.: Dominance of the Southern Ocean in anthropogenic carbon and heat uptake in CMIP5 models. J. Clim. **28**(2), 862–886 (2015). https://doi.org/10.1175/JCLI-D-14-00117.1

Fu, X., Wang, B.: The boreal-summer intraseasonal oscillations simulated in a hybrid coupled atmosphere–ocean model. Mon. Weather Rev. **132**(11), 2628–2649 (2004). https://doi.org/10.1175/MWR2811.1

Fu, X., Wang, B., Waliser, D.E., Tao, L.: Impact of atmosphere–ocean coupling on the predictability of monsoon intraseasonal oscillations. J. Atmos. Sci. **64**(1), 157–174 (2007). https://doi.org/10.1175/JAS3830.1

Gadgil, S.: The Indian monsoon and its variability. Annu. Rev. Earth Planet. Sci. **31**(1), 429–467 (2003). https://doi.org/10.1146/annurev.earth.31.100901.141251

Gao, Y., Klingaman, N.P., DeMott, C.A., Hsu, P.C.: Diagnosing Ocean feedbacks to the BSISO: SST-modulated surface fluxes and the moist static energy budget. J. Geophys. Res.-Atmos. **124**(1), 146–170 (2019). https://doi.org/10.1029/2018JD029303

Goswami, B.N., Wu, G., Yasunari, T.: The annual cycle, intraseasonal oscillations, and roadblock to seasonal predictability of the Asian summer monsoon. J. Clim. **19**(20), 5078–5099 (2006). https://doi.org/10.1175/JCLI3901.1

Goswami, B.B., Deshpande, M., Mukhopadhyay, P., Saha, S.K., Rao, S.A., Murthugudde, R., Goswami, B.N.: Simulation of monsoon intraseasonal variability in NCEP CFSv2 and its role on systematic bias. Clim. Dyn. **43**(9–10), 2725–2745 (2014). https://doi.org/10.1007/s00382-014-2458-0

Griffies, S.M., Schmidt, M.A.R.T.I.N.H., M.I.K.E.: Elements of mom4p1. GFDL Ocean Group Tech. Rep. **6**, 444 (2009)

Hallberg, R., Adcroft, A.: Reconciling estimates of the free surface height in Lagrangian vertical coordinate ocean models with mode-split time stepping. Ocean Model. **29**(1), 15–26 (2009)

Ham, Y.G., Kug, J.S., Kang, I.S., Jin, F.F., Timmermann, A.: Impact of diurnal atmosphere–ocean coupling on tropical climate simulations using a coupled GCM. Clim. Dyn. **34**(6), 905–917 (2010). https://doi.org/10.1007/s00382-009-0586-8

Hendon, H.: Air-sea interaction. In Intraseasonal Variability in the atmosphere-ocean climate system, 223–246. Springer, Berlin, Heidelberg, (2005)

Hoyos, C.D., Webster, P.J.: The role of intraseasonal variability in the nature of Asian monsoon precipitation. J. Clim. **20**(17), 4402–4424 (2007). https://doi.org/10.1175/JCLI4252.1

Hu, W.T., Li, T.: Local intraseasonal air–sea relationship over the North Indian Ocean and western North Pacific during the spring-to-summer transition. Atmospher. Ocean. Sci. Lett. **10**(1), 65–72 (2017). https://doi.org/10.1080/16742834.2017.1235463

Huang, F., Xu, Z., Guo, W.: Evaluating vector winds in the Asian-Australian monsoon region simulated by 37 CMIP5 models. Clim. Dyn. **53**(1–2), 491–507 (2019). https://doi.org/10.1007/s00382-018-4599-z

Huffman, G.J., Adler, R.F., Morrissey, M.M., Bolvin, D.T., Curtis, S., Joyce, R., McGavock, B., Susskind, J.: Global precipitation at one degree daily resolution from multisatellite observations. J. Hydrometrol. **2**(1), 36–50 (2001). https://doi.org/10.1175/1525-7541(2001)002<0036:GPAODD>2.0.CO;2

Huffman, G.J., Adler, R.F., Bolvin, D.T., Nelkin, E.J.: The TRMM multi-satellite precipitation analysis (TMPA). In Satellite rainfall applications for surface hydrology, 3–22. Springer, Dordrecht, (2010). https://doi.org/10.1007/978-90-481-2915-7_1

Jain, S., Salunke, P., Mishra, S.K., Sahany, S., Choudhary, N.: Advantage of NEX-GDDP over CMIP5 and CORDEX data: Indian summer monsoon. Atmos. Res. **228**, 152–160 (2019)

Jayasankar, C.B., Surendran, S., Rajendran, K.: Robust signals of future projections of Indian summer monsoon rainfall by IPCC AR5 climate models: role of seasonal cycle and interannual variability. Geophys. Res. Lett. **42**(9), 3513–3520 (2015)

Jena, P., Azad, S., Rajeevan, M.N.: CMIP5 projected changes in the annual cycle of Indian monsoon rainfall. Climate. **4**(1), 14 (2016)

Jiang, X., Li, J.: Influence of the annual cycle of sea surface temperature on the monsoon onset. Journal of Research Atmospheres, 116 (D10), (2011). https://doi.org/10.1029/2010JD015236

Jiang, X., Li, T., Wang, B.: Structures and mechanisms of the northward propagating boreal summer intraseasonal oscillation. J. Clim. **17**(5), 1022–1039 (2004). https://doi.org/10.1175/1520-0442(2004)017<1022:SAMOTN>2.0.CO;2

Jiang, X., Yang, S., Li, Y., Kumar, A., Liu, X., Zuo, Z., Jha, B.: Seasonal-to-interannual prediction of the Asian summer monsoon in the NCEP climate forecast system version 2. J. Clim. **26**(11), 3708–3727 (2013). https://doi.org/10.1175/JCLI-D-12-00437.1

Kadel, I., Yamazaki, T., Iwasaki, T., Abdillah, M.R.: Projection of future monsoon precipitation over the Central Himalayas by CMIP5 models under warming scenarios. Clim. Res. **75**(1), 1–21 (2018)

Kalnay, E., Kanamitsu, M., Kistler, R., Collins, W., Deaven, D., Gandin, L., Iredell, M., Saha, S., White, G., Woollen, J., Zhu, Y., Chelliah, M., Ebisuzak, W., Higgins, W., Janowiak, J., Mo, K.C., Ropelewski, C., Wang, J., Leetmaa, A., Reynolds, R., Roy, J., Joseph, D.: The NCEP/NCAR 40-year reanalysis project. Bull. Am. Meteorol. Soc. **77**(3), 437–472 (1996). https://doi.org/10.1175/15200477(1996)077<0437:TNYRP>2.0.CO;2

Kang, I.S., Kim, D., Kug, J.S.: Mechanism for northward propagation of boreal summer intraseasonal oscillation: Convective momentum transport. Geophys. Res. Lett., 37(24), (2010). https://doi.org/10.1029/2010GL045072

Karmakar, N., Krishnamurti, T.N.: Characteristics of northward propagating intraseasonal oscillation in the Indian summer monsoon. Clim. Dyn. **52**(3–4), 1903–1916 (2019). https://doi.org/10.1007/s00382-018-4268-2

Karmakar, N. and Misra, V.: Differences in Northward propagation of convection over the Arabian Sea and Bay of Bengal during boreal summer. J. Geophys. Res.-Atmos., 125(3), (2020)

Kemball-Cook, S., Wang, B.: Equatorial waves and air–sea interaction in the boreal summer intraseasonal oscillation. J. Clim. **14**(13), 2923–2942 (2001). https://doi.org/10.1175/1520-0442(2001)014<2923:EWAASI>2.0.CO;2

Kemball-Cook, S., Wang, B., Fu, X.: Simulation of the intraseasonal oscillation in the ECHAM-4 model: the impact of coupling with an ocean model. J. Atmos. Sci. **59**(9), 14331453 (2002). https://doi.org/10.1175/1520469(2002)059<1433:SOTIOI>2.0.CO;2

Kikuchi, K., Wang, B., Kajikawa, Y.: Bimodal representation of the tropical intraseasonal oscillation. Clim. Dyn. **38**(9–10), 1989–2000 (2012). https://doi.org/10.1007/s00382-011-1159-1

Klingaman, N.P., Demott, C.A.: Mean State Biases and Interannual Variability Affect Perceived Sensitivities of the Madden-Julian Oscillation to Air-Sea Coupling. J. Adv. Model. Earth Syst. **12**(2), e2019MS001799 (2020)

Klingaman, N.P., Woolnough, S.J., Weller, H., Slingo, J.M.: The impact of finer-resolution air–sea coupling on the intraseasonal oscillation of the Indian monsoon. J. Clim. **24**(10), 2451–2468 (2011). https://doi.org/10.1175/2010JCLI3868.1

Knutti, R., Sedláček, J.: Robustness and uncertainties in the new CMIP5 climate model projections. Nat. Clim. Chang. **3**(4), 369–373 (2013). https://doi.org/10.1038/nclimate1716

Konda, G., Vissa, N.K.: Intraseasonal convection and Air–Sea fluxes over the Indian monsoon region revealed from the bimodal ISO index. Pure Appl. Geophys. **176**, 3665–3680 (2019). https://doi.org/10.1007/s00024-019-02119-1

Krishnamurthy, V., Achuthavarier, D.: Intraseasonal oscillations of the monsoon circulation over South Asia. Clim. Dyn. **38**(11–12), 2335–2353 (2012). https://doi.org/10.1007/s00382-011-1153-7

Lee, J.Y., Wang, B.: Future change of global monsoon in the CMIP5. Clim. Dyn. **42**(1–2), 101–119 (2014). https://doi.org/10.1007/s00382-012-1564-0

Lee, J.Y., Wang, B., Wheeler, M.C., Fu, X., Waliser, D.E., Kang, I.S.: Real-time multivariate indices for the boreal summer intraseasonal oscillation over the Asian summer monsoon region. Clim. Dyn. **40**(1–2), 493–509 (2013). https://doi.org/10.1007/s00382-012-1544-4

Li, K., Li, Z., Yang, Y., Xiang, B., Liu, Y., Yu, W.: Strong modulations on the bay of Bengal monsoon onset vortex by the first northward-propagating intra-seasonal oscillation. Clim. Dyn. **47**(1–2), 107–115 (2016). https://doi.org/10.1007/s00382-015-2826-4

Li, K., Feng, L., Liu, Y., Yang, Y., Li, Z., Yu, W.: The northward-propagating Intraseasonal oscillations in the northern Indian Ocean during spring–early summer. J. Clim. **31**(17), 7003–7017 (2018). https://doi.org/10.1175/JCLI-D-17-0781.1

Liu, F., Wang, B., Kang, I.S.: Roles of barotropic convective momentum transport in the intraseasonal oscillation. J. Clim. **28**(12), 4908–4920 (2015). https://doi.org/10.1175/JCLI-D-14-00575.1

Liu, F., Zhao, J., Fu, X., Huang, G.: The role of shallow convection in promoting the northward propagation of boreal summer intraseasonal oscillation. Theor. Appl. Climatol. **131**(3–4), 1387–1395 (2018). https://doi.org/10.1007/s00704-017-2064-2

Nakano, M., Kikuchi, K.: Seasonality of Intraseasonal variability in global climate models. Geophys. Res. Lett. **46**(8), 4441–4449 (2019). https://doi.org/10.1029/2019GL082443

Neena, J.M., Waliser, D., Jiang, X.: Model performance metrics and process diagnostics for boreal summer intraseasonal variability. Clim. Dyn. **48**(5–6), 1661–1683 (2017). https://doi.org/10.1007/s00382-016-3166-8

Oh, J.H., Kim, B.M., Kim, K.Y., Song, H.J., Lim, G.H.: The impact of the diurnal cycle on the MJO over the maritime continent: a modeling study assimilating TRMM rain rate into global analysis. Clim. Dyn. **40**(3–4), 893–911 (2013). https://doi.org/10.1007/s00382-012-1419-8

Parthasarathy, B., Munot, A.A., Kothawale, D.R.: All-India monthly and seasonal rainfall series: 1871–1993. Theor. Appl. Climatol. **49**(4), 217–224 (1994)

Pathak, R., Sahany, S., Mishra, S.K., Dash, S.K.: Precipitation biases in CMIP5 models over the south Asian region. Sci. Rep. **9**(1), 1–13 (2019). https://doi.org/10.1038/s41598-019-45907-4

Pokhrel, S., Dutta, U., Rahaman, H., Chaudhari, H., Hazra, A., Saha, S.K., Veeranjaneyulu, C.: Evaluation of different heat flux products over the Tropical Indian Ocean. Earth Space Sci. **7**(6), e2019EA000988 (2020)

Preethi, B., Ramya, R., Patwardhan, S.K., Mujumdar, M., Kripalani, R.H.: Variability of Indian summer monsoon droughts in CMIP5 climate models. Clim. Dyn. **53**(3–4), 1937–1962 (2019)

Ramu, D.A., Chowdary, J.S., Ramakrishna, S.S.V.S., Kumar, O.S.R.U.B.: Diversity in the representation of large-scale circulation associated with ENSO-Indian summer monsoon teleconnections in CMIP5 models. Theor. Appl. Climatol. **132**(1–2), 465–478 (2018). https://doi.org/10.1007/s00704-017-2092-y

Reynolds, R.W., Smith, T.M., Liu, C., Chelton, D.B., Casey, K.S., Schlax, M.G.: Daily high-resolution-blended analyses for sea surface temperature. J. Clim. **20**(22), 5473–5496 (2007). https://doi.org/10.1175/2007JCLI1824.1

Rienecker, M.M., Suarez, M.J., Gelaro, R., Todling, R., Bacmeister, J., Liu, E., Bosilovich, M.G., Schubert, S.D., Takacs, L., Kim, G.K., Bloom, S., Chen, J., Collins, D., Conaty, A., Silva, A., Gu, W., Joiner, J., Koster, R.D., Luchesi, R., Molod, A., Owens, T., Pawson, A., Pegion, P., Redder, C.R., Reichle, R., Robertson, F.R., Ruddick, A.G., Sienkiewicz, M., Woolen, J.: MERRA: NASA's modern-era retrospective analysis for research and applications. J. Clim. **24**(14), 3624–3648 (2011). https://doi.org/10.1175/JCLI-D-11-00015.1

Roxy, M., Tanimoto, Y.: Role of SST over the Indian Ocean in influencing the intraseasonal variability of the Indian summer monsoon. J. Meteorol. Soc. Japan. Ser. II. **85**(3), 349–358 (2007). https://doi.org/10.2151/jmsj.85.349

Roxy, M., Tanimoto, Y.: Influence of sea surface temperature on the intraseasonal variability of the South China Sea summer monsoon. Clim. Dyn. **39**(5), 1209–1218 (2012). https://doi.org/10.1007/s00382-011-1118-x

Roxy, M., Tanimoto, Y., Preethi, B., Terray, P., Krishnan, R.: Intraseasonal SST-precipitation relationship and its spatial variability over the tropical summer monsoon region. Clim. Dyn. **41**(1), 45–61 (2013). https://doi.org/10.1007/s00382-012-1547-1

Sabeerali, C.T., Ramu Dandi, A., Dhakate, A., Salunke, K., Mahapatra, S., Rao, S.A.: Simulation of boreal summer intraseasonal oscillations in the latest CMIP5 coupled GCMs. J. Geophys. Res.-Atmos. **118**(10), 4401–4420 (2013). https://doi.org/10.1002/jgrd.50403

Sayantani, O., Gnanaseelan, C.: Tropical Indian Ocean subsurface temperature variability and the forcing mechanisms. Clim. Dyn. **44**(9–10), 2447–2462 (2015). https://doi.org/10.1007/s00382-014-2379-y

Sengupta, D., Ravichandran, M.: Oscillations of bay of Bengal Sea surface temperature during the 1998 summer monsoon. Geophys. Res. Lett. **28**(10), 2033–2036 (2001). https://doi.org/10.1029/2000GL012548

Sengupta, D., Goswami, B.N., Senan, R.: Coherent intraseasonal oscillations of ocean and atmosphere during the Asian summer monsoon. Geophys. Res. Lett. **28**(21), 4127–4130 (2001). https://doi.org/10.1029/2001GL013587

Seo, K.H., Wang, W.: The madden–Julian oscillation simulated in the NCEP climate forecast system model: the importance of stratiform heating. J. Clim. **23**(18), 4770–4793 (2010). https://doi.org/10.1175/2010JCLI2983.1

Seo, K.H., Schemm, J.K.E., Wang, W., Kumar, A.: The boreal summer intraseasonal oscillation simulated in the NCEP climate forecast

system: the effect of sea surface temperature. Mon. Weather Rev. **135**(5), 1807–1827 (2007). https://doi.org/10.1175/MWR3369.1

Shang, W., Ren, X., Huang, B., Cubasch, U., Yang, X.Q.: Subseasonal intensity variation of the south Asian high in relationship to diabatic heating: observation and CMIP5 models. Clim. Dyn. **52**(3–4), 2413–2430 (2019). https://doi.org/10.1007/s00382-018-4266-4

Sharmila, S., Pillai, P.A., Joseph, S., Roxy, M., Krishna, R.P.M., Chattopadhyay, R., Abhilash, S., Sahai, A.K., Goswami, B.N.: Role of ocean–atmosphere interaction on northward propagation of Indian summer monsoon intra-seasonal oscillations (MISO). Clim. Dyn. **41**(5–6), 1651–1669 (2013)

Sharmila, S., Joseph, S., Chattopadhyay, R., Sahai, A.K., Goswami, B.N.: Asymmetry in space–time characteristics of Indian summer monsoon intraseasonal oscillations during extreme years: role of seasonal mean state. Int. J. Climatol. **35**(8), 1948–1963 (2014a). https://doi.org/10.1002/joc.4100

Sharmila, S., Joseph, S., Sahai, A.K., Abhilash, S., Chattopadhyay, R.: Future projection of Indian summer monsoon variability under climate change scenario: an assessment from CMIP5 climate models. Glob. Planet. Chang. **124**, 62–78 (2014b). https://doi.org/10.1016/j.gloplacha.2014.11.004

Shinoda, T., Hendon, H.H., Glick, J.: Intraseasonal variability of surface fluxes and sea surface temperature in the tropical western Pacific and Indian oceans. J. Clim. **11**(7), 1685–1702 (1998). https://doi.org/10.1175/1520-0442(1998)011<1685:IVOSFA>2.0.CO;2

Sperber, K.R., Annamalai, H.: Coupled model simulations of boreal summer intraseasonal (30–50 day) variability, Part1: systematic errors and caution on use of metrics. Clim. Dyn. **31**, 345–372 (2008)

Sperber, K.R., Annamalai, H., Kang, I.S., Kitoh, A., Moise, A., Turner, A., Wang, B., Zhou, T.: The Asian summer monsoon: an intercomparison of CMIP5 vs. CMIP3 simulations of the late 20th century. Clim. Dyn. **41**(9–10), 2711–2744 (2013). https://doi.org/10.1007/s00382-012-1607-6

Taylor, K.E.: Summarizing multiple aspects of model performance in a single diagram. J. Geophys. Res.-Atmos. **106**(D7), 7183–7192 (2001). https://doi.org/10.1029/2000JD900719

Taylor, K.E., Stouffer, R.J., Meehl, G.A.: An overview of CMIP5 and the experiment design. Bull. Am. Meteorol. Soc. **93**(4), 485–498 (2012). https://doi.org/10.1175/BAMS-D-11-00094.1

Thadathil, P., Muraleedharan, P.M., Rao, R.R., Somayajulu, Y.K., Reddy, G.V., Revichandran, C.: Observed seasonal variability of barrier layer in the Bay of Bengal. J. Geophys. Res. Oceans, 112(C2), (2007). https://doi.org/10.1029/2006JC003651

Thadathil, P., Thoppil, P., Rao, R.R., Muraleedharan, P.M., Somayajulu, Y.K., Gopalakrishna, V.V., Murtugudde, R., Reddy, G.V., Revichandran, C.: Seasonal variability of the observed barrier layer in the Arabian Sea. J. Phys. Oceanogr. **38**(3), 624–638 (2008). https://doi.org/10.1175/2007JPO3798.1

Vecchi, G.A., Harrison, D.E.: Monsoon breaks and subseasonal sea surface temperature variability in the bay of Bengal. J. Clim. **15**(12), 1485–1493 (2002)

Vissa, N.K., Satyanarayana, A.N.V., Prasad Kumar, B.: Comparison of mixed layer depth and barrier layer thickness for the Indian Ocean using two different climatologies. Int. J. Climatol. **33**(13), 2855–2870 (2013). https://doi.org/10.1002/joc.3635

Wang, B., Xie, X.: A model for the boreal summer intraseasonal oscillation. J. Atmos. Sci. **54**(1), 72–86 (1997). https://doi.org/10.1175/1520-0469(1997)054<0072:AMFTBS>2.0.CO;2

Wang, W., Chen, M., Kumar, A.: Impacts of ocean surface on the northward propagation of the boreal summer intraseasonal oscillation in the NCEP climate forecast system. J. Clim. **22**(24), 6561–6576 (2009). https://doi.org/10.1175/2009JCLI3007.1

Wang, C., Zhang, L., Lee, S.K., Wu, L., Mechoso, C.R.: A global perspective on CMIP5 climate model biases. Nat. Clim. Chang. **4**(3), 201–205 (2014). https://doi.org/10.1038/nclimate2118

Wang, T., Yang, X.Q., Fang, J., Sun, X., Ren, X.: Role of air–sea interaction in the 30–60-day boreal summer intraseasonal oscillation over the western North Pacific. J. Clim. **31**(4), 1653–1680 (2018). https://doi.org/10.1175/JCLI-D-17-0109.1

Webster, P.J., Magana, V.O., Palmer, T.N., Shukla, J., Tomas, R.A., Yanai, M.U., Yasunari, T.: Monsoons: processes, predictability, and the prospects for prediction. J. Geophys. Res. Oceans. **103**(C7), 14451–14510 (1998). https://doi.org/10.1029/97JC02719

Webster, P.J., Bradley, E.F., Fairall, C.W., Godfrey, J.S., Hacker, P., Houze Jr., R.A., Lukas, R., Serra, Y., Hummon, J.M., Lawrence, T.D.M., Russell, C.A.: The JASMINE pilot study. Bull. Am. Meteorol. Soc. **83**(11), 1603–1630 (2002). https://doi.org/10.1175/BAMS-83-11-1603

Webster, P.J.: Mechanisms of monsoon low-frequency variability: Surface hydrological effects. Journal of Atmospheric Sciences. 40(9), 2110–2124 (1983). https://doi.org/10.1175/1520-0469(1983)040<2110:MOMLFV>2.0.CO;2

Woolnough, S.J., Slingo, J.M., Hoskins, B.J.: The relationship between convection and sea surface temperature on intraseasonal timescales. J. Clim. **13**(12), 2086–2104 (2000). https://doi.org/10.1175/1520-0442(2000)013<2086:TRBCAS>2.0.CO;2

Wu, R.: Subseasonal variability during the South China Sea summer monsoon onset. Clim. Dyn. **34**(5), 629–642 (2010). https://doi.org/10.1007/s00382-009-0679-4

Wu, R., Kirtman, B.P., Pegion, K.: Local air–sea relationship in observations and model simulations. J. Clim. **19**(19), 4914–4932 (2006)

Xie, P., Arkin, P.A.: Global precipitation: a 17-year monthly analysis based on gauge observations, satellite estimates, and numerical model outputs. Bull. Am. Meteorol. Soc. **78**(11), 2539–2558 (1997). https://doi.org/10.1175/1520-0477(1997)078<2539:GPAYMA>2.0.CO;2

Yang, W., Seager, R., Cane, M.A., Lyon, B.: The annual cycle of east African precipitation. J. Clim. **28**(6), 2385–2404 (2015). https://doi.org/10.1175/JCLI-D-14-00484.1

Yang, B., Zhang, Y., Qian, Y., Song, F., Leung, L.R., Wu, P., Guo, Z., Lu, Y., Huang, A.: Better monsoon precipitation in coupled climate models due to bias compensation. npj Clim. Atmospher. Sci. **2**(1), 1–8 (2019a)

Yang, Y.M., Wang, B., Lee, J.Y.: Mechanisms of northward propagation of boreal summer intraseasonal oscillation revealed by climate model experiments. Geophys. Res. Lett. **46**(6), 3417–3425 (2019b)

Zhang, G.J., Mcphaden, M.J.: The relationship between sea surface temperature and latent heat flux in the equatorial Pacific. J. Clim. **8**(3), 589–605 (1995). https://doi.org/10.1175/1520-0442(1995)008<0589:TRBSST>2.0.CO;2

Zhang, L., Han, W., Li, Y., Maloney, E.D.: Role of North Indian Ocean Air–Sea interaction in summer monsoon Intraseasonal oscillation. J. Clim. **31**(19), 7885–7908 (2018). https://doi.org/10.1175/JCLI-D-17-0691.1